A study on branched fiber network sensing utilizing Brillouin scattering and its application to the remote testing of telecommunication equipment

September 2017,

Chihiro Kito

Shimane University

Interdisciplinary Graduate School of Science and Engineering

Contents

1 Introduction

1.1 Background

1.1.1 Structural health monitoring

Many of the social infrastructures such as bridges and tunnels constructed during the period of high economic growth in Japan are about to reach the end of their useful lives, and the importance of inspecting those old infrastructures is increasing. Meanwhile, there has also been a serious reduction in the labor force responsible for inspection work. The development of structural health monitoring (SHM) technology to realize the efficient inspection of these social infrastructures has been long expected.

In terms of SHM, research on optical sensing technology capable of collecting monitoring information remotely has been actively pursued [1-1, 1-2, 1-3]. An optical measurement technique utilizing stimulated Brillouin scattering, which is one of the nonlinear phenomena in optical fibers, allows the highly sensitive measurement of temperature or strain changes in a fiber under test (FUT) affixed to a sensed object [1-4]. The approach is therefore attracting attention as a promising candidate for SHM. With respect to Brillouin optical time domain analysis (BOTDA), which is a representative distributed measurement technique utilizing Brillouin scattering, various aspects of measurement performance such as spatial resolution [1-5, 1-6], measurement accuracy [1-7], sensitivity, and measured distance [1-8] have been improved in previous studies.

However, with BOTDA, it is essential to affix an FUT to a sensed object with a unicursal topology, so the wiring scalability is very poor, and the monitoring system cannot work when the affixed optical fiber is suffering from any type of optical failure

at a time of emergency. The sensing optical fiber should be wired flexibly and effectively according to the shape of the sensed object, and continuous long-term operation is strongly required even under harsh environments, including during an emergency. Therefore, it is necessary to improve the wiring scalability and reliability of optical sensing systems utilizing Brillouin scattering. Reducing the initial cost is also an important issue in terms of promoting SHM technology. Optical sensing technology utilizing Brillouin scattering such as BOTDA requires precise frequency control, and so it has been difficult to simplify the system configuration. However, by simplifying the system, we can expect to reduce the initial cost. Furthermore, if it were possible to capture the dynamic change in strain caused by the vibration of the optical fiber, the sensing application would be expanded, because a natural vibration mode measurement is useful for directly diagnosing structural deterioration [1-9].

1.1.2 Remote monitoring of optical access network

In Japan, the construction of the optical communication infrastructure is almost complete, and the quality with which large-scale facilities are maintained is very important to telecommunication carriers. Furthermore, as the facility maintenance labor force will decrease in the telecommunications industry in the near future, it is an urgent matter to develop remote testing technology that can determine a facility's status from a central office in real time. With the development of remote testing technology, we can expect the efficiency of maintenance operations to be improved, for example onsite operation will be reduced.

Optical time domain reflectometry (OTDR) has already been put into practical use as a remote testing technology. However, when an optical splitter is installed in an access network, since the backscattered signals from the branched fibers below the splitter overlap at the trunk fiber, it is difficult to locate the fault in the fiber from the central office with OTDR. And so, the reduction in maintenance operations realized by using OTDR remote testing has remained limited. On the other hand, most of the widely used fiber-to-the-home (FTTH) optical networks employ passive optical networks (PON) with an outdoor splitter. Therefore, remote testing technology beyond the splitter has been strongly requested by the telecommunication industry. Various schemes have been proposed [1-10, 1-11, 1-12, 1-13] for realizing the remote testing of branched fibers, but reference data are needed [1-10, 1-11], or it is necessary to insert additional items with different frequency characteristics into the branches in the existing optical access network [1-12, 1-13]. This issue prevents the techniques from being introduced in actual networks.

In recent years, a novel technique has been proposed to overcome the issue called end-reflection assisted Brillouin analysis (ERA-BA) [1-14, 1-15], which can measure the optical properties of branched fibers individually from a central office. This is loss measurement technology that can be introduced directly into existing optical access networks without any additional components. The ERA-BA is a method using Brillouin gain analysis that is undertaken by employing a collision between a reflected probe pulse from the far end of a branch and a pump pulse. Before this approach can put to practical use, its performance in the field should be clarified by testing it using a constructed access network as a test bed. In addition, we must consider the applicability to various fault scenarios such as faults caused by broken fibers.

1.2 Objective

The purpose of this thesis is to improve the wiring scalability and reliability of optical fiber sensing technology by making it compatible with a branched topology. Furthermore, we apply the basic principle to communication networks and clarify the performance as the PON branch remote testing.

In general, optical fiber sensing technology makes it possible to measure changes in various parameters under harsh environments by taking advantage of the characteristics of optical fibers, namely resistance to weather, extreme heat and explosions, flexibility, and non-inductivity to electromagnetic noise. As mentioned in Section 1.1.1, Brillouin fiber sensing technology measures changes in the temperature or strain of an FUT by attaching it to a sensed object with a unicursal topology. In other words, there is a dilemma resulting from the fact that the sensing function is immediately lost when the attached optical fiber is broken by a large parameter change while emergency monitoring is underway in a harsh environment. Furthermore, since the sensing system only allows a unicursal topology, it has poor expandability. Once the optical fiber is attached to a sensed object, it requires considerable operational cost to expand wiring routes or make trivial changes.

This thesis first describes a distributed optical sensing technique for a branched topology designed to improve the wiring scalability and reliability of optical sensing systems. By undertaking sensing on a branched sensing network, unlike with a unicursal topology, even if a single branch is broken, monitoring can continue by using other branches. Furthermore, by adding optical splitters to the network, it is possible to extend the sensing area easily at any time.

However, if a branched optical network is adopted for the sensing topology, there is concern that the sensitivity will decrease due to an additional branching loss. In this thesis, in addition to dealing with a branched optical network, I propose a method that employs a time division multiplexed test pulse to increase sensitivity. And then, I clarify the figure of merit (FoM) of the proposed method for a traditional BOTDA. By showing the superior sensitivity of the proposed method compared with BOTDA in cases with practical system parameters (number of branches and measurement distance), I prove the wide applicability of the branched fiber sensing technique with highly robustness and easy expandability.

The optical sensing technology for the branched topology mentioned above is technically based on end-reflection assisted Brillouin analysis (ERA-BA), which is proposed as a technique for measuring the individual properties of branched optical fibers. If ERA-BA can be put to practical use as a method for testing PONs remotely, telecommunication carriers will be able to determine the state of all their communication media including the branches in real time. Thanks to the fact that all testing is accomplished remotely, the number of on-site maintenance operations can be greatly reduced. In this thesis, I describe a PON monitoring field trial with ERA-BA, and confirm the basic operation in an actual installation environment. In addition, I accumulate statistical data regarding branch length in the field to make it possible to set the target performance of the spatial and branch identification resolution of the practical system. I also clarify the applicability of ERA-BA to a fiber broken fault, which is a major factor in optical communication failure.

Various optical measurement technologies using Brillouin scattering have been proposed [1-17], but practical use cases have not progressed other than in specific

industries such as plant field introducing temperature or strain monitoring. To spread the use of an optical measurement system using Brillouin scattering as SHM technology, it is essential that we greatly reduce the cost of the sensing equipment. Moreover, if it were also possible to measure the natural vibration mode, which directly reflects structural deterioration, the applications would be greatly extended to various industries with a potential need for SHM technology. In this thesis, my aim is to diversify the optical sensing applications by establishing a vibration sensing technique utilizing stimulated Brillouin scattering with a simplified system setup.

As mentioned in the above three paragraphs, this thesis focuses on the following three points.

(A) A novel optical fiber sensing technology supporting branched fiber topology designed to improve the reliability and wiring scalability of sensing systems

(B) An ERA-BA field trial designed to evaluate the practicality of the remote testing of PON branches and its applicability to fiber broken fault

(C) A vibration measurement technique with a simplified system setup designed to spread the use of Brillouin sensing technology

Thus, this thesis contributes to the development of optical fiber sensing technology utilizing Brillouin scattering and its application to remote testing in the telecommunication industry.

1.3 Outline

As shown in Figure 1-1, this thesis has 6 chapters. Each chapter is summarized below.

The first chapter is an introduction that provides the research background, objectives, and outline of this thesis.

Chapter 2 describes the principle of ERA-BA, which is a recently proposed method supporting branched fiber topology with Brillouin gain analysis. The main body of this thesis develops a measurement method supporting a branched topology based on ERA-BA designed to establish highly reliable fiber sensing and useful remote testing of optical communication networks.

Chapter 3 proposes a branched optical fiber sensing technique based on ERA-BA using time division multiplexed probe pulses, mainly for temperature/strain measurement. With optical sensing technology corresponding to a branched optical network, reliability and wiring scalability can be greatly enhanced for a conventional unicursal topology system. In addition, from the viewpoint of sensitivity, the proposed branched fiber sensing technique is compared with conventional BOTDA. As a result, the proposed technique shows excellent sensitivity with most practical system parameters (number of branches and distance range) despite the additional branched optical loss. This is the most important result of this thesis.

In chapter 4, I apply ERA-BA as a remote testing technique for optical access networks as described in chapter 2. A prototype of ERA-BA system is designed for a field trial, and its basic function is confirmed in the field. Since information such as the branch length distribution and the dispersion of the Brillouin gain spectrum are needed

to define the target performance of the equipment, these statistical data are obtained by performing a sampling survey with in-service PONs. Furthermore, field trial results are described in which the individual branch loss distribution of the installed PON was measured for the first time using the ERA-BA prototype equipment. There are also many cases of fiber breakage causing optical communication failure. Since the proposed principle is strongly related to the return loss of the far end, the measurement sensitivity varies depending on the broken state of the fiber. I investigate the return loss probability when the optical cable is broken, and also report a branched fiber loss measurement obtained with a broken fiber edge.

In Chapter 5, I propose a novel method that both simplifies the sensing system configuration and increases the measurement speed of Brillouin sensing technology, including ERA-BA. With the proposed method, by using a frequency-swept test pulse for BOTDA, a convex Brillouin gain implying a Brillouin frequency shift (BFS) is observed on a probe pulse in the time domain. The principle behind the frequency-swept test pulse is that it quickly acquires BFS and has a simplified system configuration without precise frequency control. As a result, we can expect the method to be applied to the dynamic strain monitoring of structures, such as the measurement of the natural vibration mode.

Chapter 6 provides the conclusion to this thesis by summarizing the main results obtained in this work.

In conclusion, this thesis contributes to the development of SHM technology with excellent reliability and wiring scalability, and constitutes a step towards the practical use of remote testing for existing PONs with branch topology, thus contributing to maintenance efficiency. Furthermore, it can be expected to expand the applicable field

of the optical fiber sensing by proposing a novel Brillouin sensing method that supports vibration sensing and reduces the equipment cost of a measurement system utilizing stimulated Brillouin scattering.

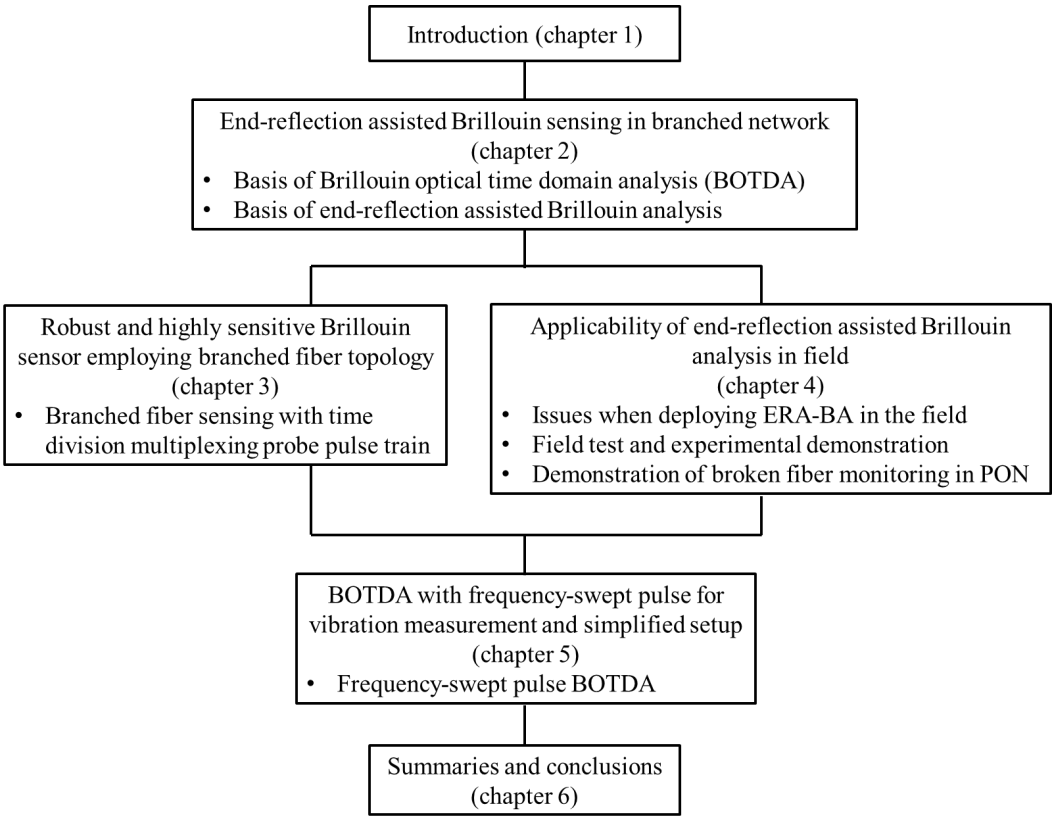

Fig.1-1 Thesis organization.

2 End-reflection assisted Brillouin sensing in branched network

2.1 Introduction

Optical fiber sensing technology utilizing Brillouin scattering can measure changes in temperature or strain with high sensitivity by using the dependence of those parameters on the Brillouin frequency shift (BFS). Various methods have been proposed that can measure changes in Brillouin scattering with the aim of using them to monitor the health of social infrastructures such as dams, tunnels, bridges and high-rise buildings [2-1]. Brillouin optical time domain analysis (BOTDA), which is a typical such technique, was proposed in 1989 [2-2]. Subsequently, all aspects of measurement performance including spatial resolution [2-3, 2-4], measurement accuracy [2-5], sensitivity, and measurement distance [2-6], have been actively studied and the approach has been widely recognized as a distributed sensing technique for temperature and strain change. On the other hand, BOTDA was originally developed as a nondestructive technique for measuring optical fiber loss by measuring the Brillouin gain intensity [2-7].

End-reflection assisted Brillouin analysis (ERA-BA) has recently been proposed [2-8, 2-9], which can measure the individual characteristics of branched fibers based on BOTDA. ERA-BA measures the branched fiber characteristics by analyzing the Brillouin gain caused by a collision between a pump pulse and a probe pulse reflected from the far end of the branch. The branched fiber measurement technique with

ERA-BA enables the remote testing of all optical access networks that include branched fibers, and greatly reduces the number of on-site operations. It can be expected to provide the high quality maintenance of extremely large network facilities at a low cost and with a small labor force.

In this thesis, I study optical fiber sensing technology that provides high reliability and wiring scalability corresponding to a branched network based on ERA-BA. I also study the practicality of ERA-BA as a remote testing method for telecommunication networks with a splitter, i.e. passive optical networks (PONs), in an actual installed environment.

This chapter outlines the basic techniques used in this work, namely BOTDA and ERA-BA. Section 2.2 describes the basic principle of BOTDA. Section 2.3.1 describes the principle and applicable conditions for ERA-BA. Furthermore, section 2.3.2 describes the expected impact of introducing the remote testing of PON branches using the conventional telecommunication facility maintenance scheme as an example.

2.2 Basis of Brillouin optical time domain analysis (BOTDA)

2.2.1 Brillouin sensing mechanism

The optical measurement technique utilizing Brillouin scattering is a method that employs the linear dependence of the Brillouin frequency shift (BFS) on temperature or strain change. To determine the BFS, the peak frequency of the Brillouin gain spectrum (BGS) is observed with a fitting function. Brillouin scattering is the inelastic scattering of photons by acoustic phonons, and Brillouin scattering downshifts light frequency as shown by Eq. 2-2-1.

$$\nu_{\mathrm{B}} = {2n\mathrm{v}_{\mathrm{A}}}\Big/{\lambda_u} \tag{2-2-1}$$

Here, ν_B is the BFS, n is the refractive index of the medium, v_A is the sound velocity, and λ_u is the wavelength of the pump light. For a silica optical fiber (refractive index n: 1.45), with a sound velocity v_A of 5.96 km/s, the frequency shift caused by Brillouin scattering in the 1.55 μm wavelength band is approximately 11.1 GHz [2-10].

Brillouin sensing techniques monitor the linear increase in BFS that occurs with increases in temperature [2-11] or tensile strain [2-12]. This dependence is due to the fact that the sound velocity in the optical fiber varies depending on temperature and strain. Equations 2-2-2 and 2-2-3 express the dependence of BFS on temperature and tensile strain, respectively.

$$\nu_{\mathrm{B}}(t) = \nu_B(\mathrm{t_r})\left[1 + C_t(t - t_r)\right] \tag{2-2-2}$$

$$\nu_{\mathrm{B}}(\varepsilon) = \nu_B(0)\left[1 + C_s\varepsilon\right] \tag{2-2-3}$$

Here, t is the temperature, t_r is the reference temperature, and ε is the tensile strain. C_t and C_s are linear coefficients for changes in temperature and strain of 1.10 MHz/°C and

0.0483 MHz/με, respectively, at a wavelength of 1553.8 nm [2-13]. With Brillouin sensing technology, since the temperature and strain changes cannot be measured separately, the BFS change $\delta\nu_B$ is sometimes expressed as Eq. 2-2-4.

$$\delta\nu_{\mathrm{B}}(t,\varepsilon) = C_t\delta t + C_\varepsilon\delta\varepsilon \tag{2-2-4}$$

Here, δt and $\delta\varepsilon$ are changes in temperature and strain, respectively. In practice, to compensate for changes in temperature or strain not intended for measurement, a reference optical fiber or reference data are prepared.

2.2.2 Minimum detectable BFS change and spatial resolution

In general, fitting is applied to the obtained BGS to determine the BFS. The BGS has a shape that can be approximated by the Lorentz function with the center frequency at ν_B and a full width at half maximum of $\Delta\nu_B$. When quadrature fitting is applied to the full width at half maximum of the BGS, the measurement error of the BFS, namely the minimum sensitivity of the BFS change, can be estimated with Eq. 2-2-5 [2-14].

$$\sigma_\nu(z) = \frac{1}{SNR(z)}\sqrt{\frac{3}{4}\delta \cdot \Delta\nu_B} \tag{2-2-5}$$

Here, SNR(z) is the signal-to-noise ratio (SNR) of the BGS peak at position z, and δ is the frequency sample step ($\delta << \Delta\nu_B$). Eq. 2-2-5 shows that the detectable minimum BFS change decreases in inverse proportion to the SNR of the measured BGS distribution, and increases in proportion to the square root of the frequency sample step δ.

Brillouin optical time domain analysis (BOTDA) measures the Brillouin scattering intensity as a function of time. When the response speed of the photo receiver is sufficiently high, the spatial resolution corresponds to the pulse width of the pump light. The spatial resolution δz is expressed by Eq. 2-2-6 [2-15].

$$\delta z = {}^{vW_u}\!/_{2} \tag{2-2-4}$$

Here, v is the group velocity of light in the optical fiber, and W_u is the pulse width of the pump light. The spatial resolution of the standard BOTDA is limited to 1 m. This is because the phonon lifetime is about 10 ns and it is difficult to realize a pump pulse width of less than 1 m.

2.2.3 System setup for Brillouin optical time domain analysis

To measure the BFS along a sensing fiber, it is necessary to obtain the BGS distribution as the frequency dependence of the Brillouin gain intensity. Figure 1 shows a conventional BOTDA system. Generally, the pump light is pulsed light, and the probe light is launched from the opposite side by using a continuous beam. And Brillouin interaction occurs during the collision of the test beams in the fiber under test (FUT). The laser output is divided by a coupler to form a pump light and a probe light. To generate a Brillouin interaction between the test beams, the probe light frequency is downshifted with an optical frequency shifter by the BFS (approximately 11 GHz at a 1.55 μm wavelength). The pump light is pulsed by a pulse shaper such as an electro-optic modulator, an acousto-optic modulator, or a semiconductor optical amplifier. To eliminate the polarization dependence of the Brillouin gain, a polarization scrambler or polarization switch is inserted in the optical path of the pump or probe light. While sequentially changing the frequency offset by using the frequency shifter, it scans in the vicinity of the BFS of the FUT. The Rayleigh scattering of the pump light, which is an unnecessary signal component, can be eliminated with a narrow linewidth optical filter such as a fiber Bragg grating (FBG). The Brillouin gain spectrum distribution can be obtained with the above measurement system.

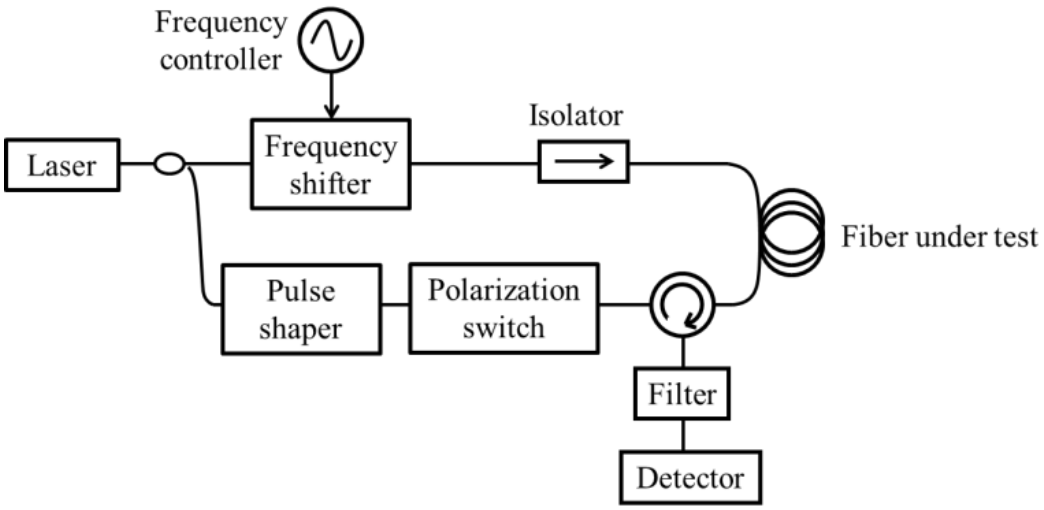

Fig. 2-1 Basic setup for BOTDA.

2.3 Basis of end-reflection assisted Brillouin analysis (ERA-BA)

This section outlines the principle of ERA-BA. ERA-BA is a unique measurement technique that is compatible with branched fiber topology. In other words, it is possible to measure the characteristics of the optical fiber for each branch connected to the optical splitter by using Brillouin gain analysis. In this thesis, by further developing ERA-BA, I aim to realize a highly robust branched fiber sensing and remote testing technology for PON branches.

2.3.1 Principle

Figure 2 is a schematic illustration showing the principle of ERA-BA. ERA-BA is an optical measurement technique that measures the characteristics of each branched fiber from the trunk fiber side. Here, the characteristics are the optical loss, and changes in temperature and strain. The branched fiber characteristics are measured by Brillouin gain analysis by employing the collision between the pump pulse and the probe pulse returning from the far end of the branch. The dependence of the Brillouin gain intensity on the pump power is useful for measuring branch loss. Meanwhile, the BFS, which varies depending on changes in temperature and strain, is measured for optical fiber sensing with branched fiber topology.

To cause the test pulses to collide in the branched fibers, we need an optical filter that reflects the probe pulse at the far end of the branched fiber. The pump pulse is launched after the probe pulse with a time delay of Δt to collide at a position $v\Delta t/2$ from the far end. A distribution measurement is possible by sequentially changing the time delay Δt. To generate far-end reflection effectively in an existing access network, we

can use a test light cut-off filter as recommended in ITU-T L.66 [2-16]. On the other hand, with branched fiber sensing, we can use an FBG filter or a total reflection filter designed for the probe wavelength.

The round trip time difference of the returned probe pulses caused by the different lengths of the branched fibers is used to determine the signals from a branched fiber. To identify the branched fibers, we at least need the branch length difference δL expressed by Eq. 2-3-1. This is called the branch identification resolution.

$$\delta L = {vW_r}/{2} \tag{2-2-4}$$

W_r is the probe pulse width. For telecommunication networks, since the branched fiber lengths differ randomly by several meters, the target performance of the fiber identification resolution should be equal to or higher than that value. Statistical data for branch length difference collected in the field are shown in Section 4. With branched fiber sensing, the branch length difference can be arbitrarily set by using an extra delay fiber. Note that the spatial resolution can be defined by Eq. 2-2-4 using the pump pulse width as with conventional BOTDA.

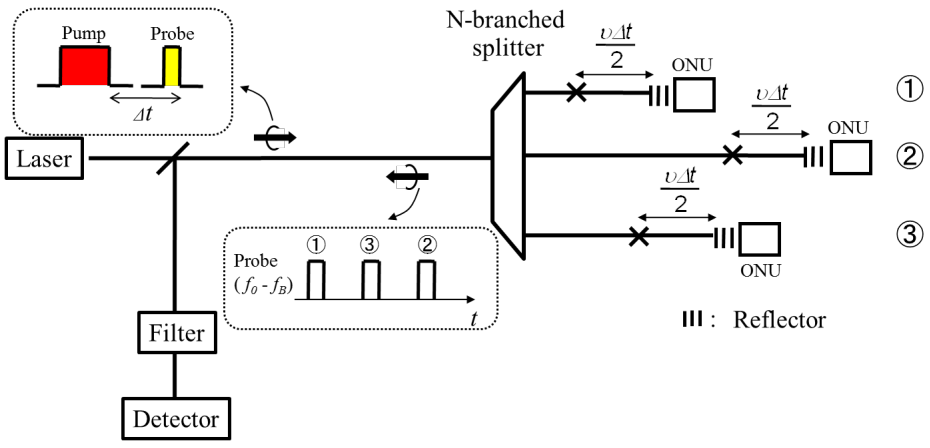

Fig. 2-2 Schematic illustration of principle of ERA-BA.

2.3.2 Application to remote monitoring of optical access network

When ERA-BA is developed as a loss distribution measurement technique for use with a branched optical fiber, it is expected that it will be widely used as a remote testing technology for PON branches in the telecommunication industry. This section explains the changes made to the maintenance scheme when a PON monitoring technique such as ERA-BA is put into practical use.

In general maintenance operation schemes, optical faults in access networks are often detected thanks to a user's failure report. When a failure is suspected in an optical fiber, a trunk cable loss measurement is undertaken from a central office using optical time domain reflectometry (OTDR) to first isolate the failure location. If an irregular loss is found on the trunk cable, the maintenance operator travels directly to repair the failure. On the other hand, if the soundness of the trunk optical cable is guaranteed by the OTDR test, a branched fiber fault will be strongly suspected. Since it is difficult to determine the state of the system beyond the optical splitter from the office, operators travel to the user’s premises, and an OTDR test is performed from the optical network unit (ONU) side to identify the fault location on the branched fiber [2-17]. In the present scheme, there is a problem in that fault location and recovery work on the branched fiber is influenced by the user's home situation, and it is impossible to realize efficient maintenance led by the communication carrier.

If we can realize the remote testing of branched fibers, it will be possible to confirm the soundness of all the optical communication media including beyond the splitter from the central office. In other words, there is no need to disturb the user at home at the time of a fiber failure because the communication carriers can understand the condition

of the facilities and determine a maintenance schedule. In addition, when the soundness of the trunk and branched fiber is guaranteed, an ONU failure can be strongly suspected, so the maintenance operation can be completed simply by mailing an ONU to the user reporting the failure. Furthermore, by conducting periodic testing of the entire optical access network using the PON branch monitoring technique, there is the possibility that age related deterioration in fiber loss can be detected. As a result, a facility renewal and maintenance operation can be carried out systematically before the communication link fails. As described above, the maintenance operation cost for a huge number of network facilities would be greatly reduced by enabling the remote testing of branched fiber.

2.4 Conclusion

Chapter 2 outlined BOTDA, which is a representative optical measurement technology utilizing Brillouin gain analysis. This thesis describes an optical fiber sensing technology that uses Brillouin scattering, which can measure temperature and strain changes with high sensitivity, from the viewpoint of its compatibility with branch topology, the simplification of the system configuration, and dynamic strain measurement. In addition, the basic principle of ERA-BA as the technical basis of this thesis was described in this chapter. ERA-BA is a distributed measurement technology that can be employed with branched fiber topology. I described the efficient maintenance scheme that is realized when ERA-BA is put to practical use for remote PON branch monitoring in the telecommunications industry. In chapter 3 and subsequent chapters I discussed an investigation designed to realize optical sensing technology for use with a branched fiber topology and the remote testing of PONs by further developing ERA-BA.

3 Robust and highly sensitive Brillouin sensor employing branched fiber topology

3.1 Introduction

The distributional analysis of stimulated Brillouin scattering has been widely investigated by using time domain [3-1]-[3-3] and correlation domain analysis [3-4] with a view to observing strain and/or temperature variations induced in optical fibers. Conventionally, in such technologies, sensing points are unicursally connected with a single optical fiber, even when the sensed area extends in two or three dimensions (Fig. 3-1(a)). With the conventional sensing fiber topology, it is difficult to expand the sensed area flexibly. Moreover, a single fiber fault causes the entire sensing system to shut down. To overcome this problem, a branched fiber configuration with a passive power splitter was proposed to improve network reliability and provide configuration flexibility [3-5]. However, the approach involved allocating different Brillouin frequency shifts to each branch by changing such material properties of the fibers as the dopant concentration, and so standard optical fibers could not be employed. A simplified branched fiber sensing technique with one sort of branched fiber is expected to be suitable for temperature/strain sensing, e.g. in data center or civil structure monitoring, by utilizing its flexible scalability and high reliability (Fig. 3-1(b)).

Recently, a novel technology called “end-reflection assisted Brillouin analysis (ERA-BA)” was proposed, which employs a passive splitter to distribute a probe signal to branches, and distinguishes between individual branches simply by using their length

differences [3-6], [3-7]. With this technique, a single pair of pump and probe pulses yields a Brillouin interaction at a single point when test pulses are launched. While the technology has been presented for monitoring so called passive optical networks (PONs) deployed in optical access networks, it can be straightforwardly applied to the Brillouin sensing mentioned in the previous paragraph, without any intentional allocation of the Brillouin frequencies, yield robustness and flexibility of the system thanks to its branched fiber topology.

However, the issue of sensitivity, or dynamic or distance range of the system has not yet been addressed. Intuitively, the insertion of the passive splitter causes significant optical losses when the light goes in the both directions, so that the system should pay some penalty to achieve distance range that is equivalent to that of the conventional unicursal systems. The purpose of the last section of this chapter is to discuss the applicable range of the proposed system.

In this chapter, a novel probe signal design for end-reflection assisted Brillouin analysis was presented to enhance the energy efficiency of the measurement while still employing time domain analysis, and thus maintaining system simplicity [3-8]. After describing the principle (section II) and an experimental demonstration (section III), author compares the proposed system with a branch topology with the conventional Brillouin time domain analysis (BOTDA) system with a unicursal fiber topology, and show that a simulation implies a superior sensing signal-to-noise ratio to that of BOTDA for whole surface monitoring in spite of the disadvantage of the branched loss. Author believes the proposed branched fiber sensing technology would be particularly useful for application to a temperature and strain sensor with a very robust and flexible topology.

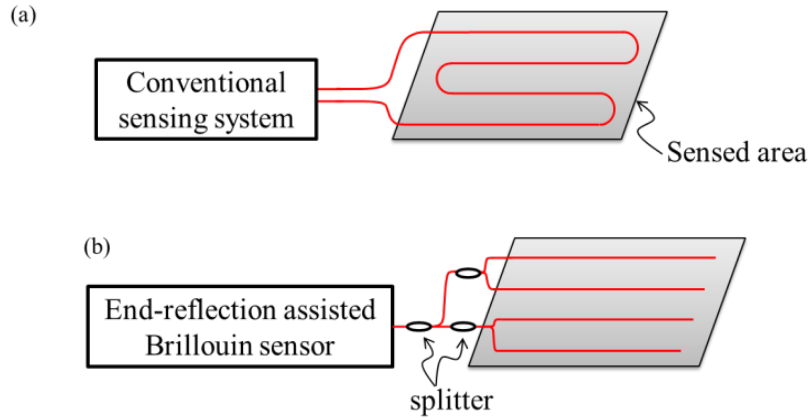

Fig. 3-1. Illustration of sensing fiber topology (a) a unicursal topology for conventional sensing technique such as BOTDA (b) a branch topology for the proposed technique.

3.2 Branched fiber sensing with time division multiplexing probe pulse train

Fig. 3-2(a) shows the proposed Brillouin analysis configuration for monitoring branched optical fiber. The sensor fiber consists of a passive power splitter and N branches with end reflectors in every branch. To describe the configuration, let the lengths of the branches with respect to the shortest branch be $0<\tau_1<\tau_2$, —, $<\tau_{N-1}$. And the τ_i values are written in terms of the roundtrip times to the end of each branch. The total branched sensing range is assumed to be T.

The technology proposed here uses a series of probe pulses and a single pump pulse, instead of a single pair of probe and pump pulses. The probe beam consists of a series of pulses with a pulse width of $\Delta\tau_{pro}$, a repetition interval of ΔT, and a train length that nearly equals the entire sensing range, T. Hence, the number of launched probe pulses is about $T/\Delta T$. A single pump pulse with a Brillouin frequency shift (BFS) accompanies the probe pulse train with an interval of Δt after the last probe pulse. The probe pulses are reflected by the end reflectors in each branch, and the m-th probe pulse collides with the pump pulse and acquires the Brillouin gain at a distance of $v_g(\Delta t+m\Delta T)/2$ from the end reflectors in every branch, where v_g is the light velocity and m is an integer ($0 \le m \le T/\Delta T$). The entire range, T, can be analyzed by scanning Δt from 0 to ΔT (instead of scanning the entire range, T).

To determine the Brillouin gains yielded in the branches individually, the probe pulses, which are recombined at the splitter, must not overlap each other. In other words, the probe pulses from different branches must be located in different time slots. With some length manipulation of the branches, this condition can be realized in a

straightforward manner as shown in Fig. 3-2(b). Set the probe pulse interval ΔT at $N\Delta\tau_{pro}$. Then, the probe pulses from the i-th branch are located at $m\Delta T+\tau_i$. The necessary and sufficient condition for avoiding any overlapping of the probe pulses is that all of the remainders of the branch lengths, τ_i, when they are divided by ΔT, shall be different from each other. This condition can be realized by manipulating the branch length, and the required manipulation range is always less than ΔT.

The described technology enhances the data collection rate, or reduces the data collection time, by a factor of $\sim_{T/\Delta T}$, by comparison with the previously investigated single pair probe-pump scheme. Also, to increase the data collection rate, author proposes a fiber sensor design that employs different BFS fibers for the feeder and branched fibers. Since no Brillouin interaction occurs on the feeder fiber, the test beam repetition rate (data collection rate) is decided solely by the roundtrip time of the longest branched fiber (excluding the roundtrip time of the feeder fiber). Additionally, in terms of pump depletion, the effect does not occur in feeder fiber. To benefit from the use of different BFS fibers in the sensing fiber topology, the difference between the BFSs of the feeder and branched fibers should be designed to be sufficiently wider than the expected BFS change caused by temperature or strain.

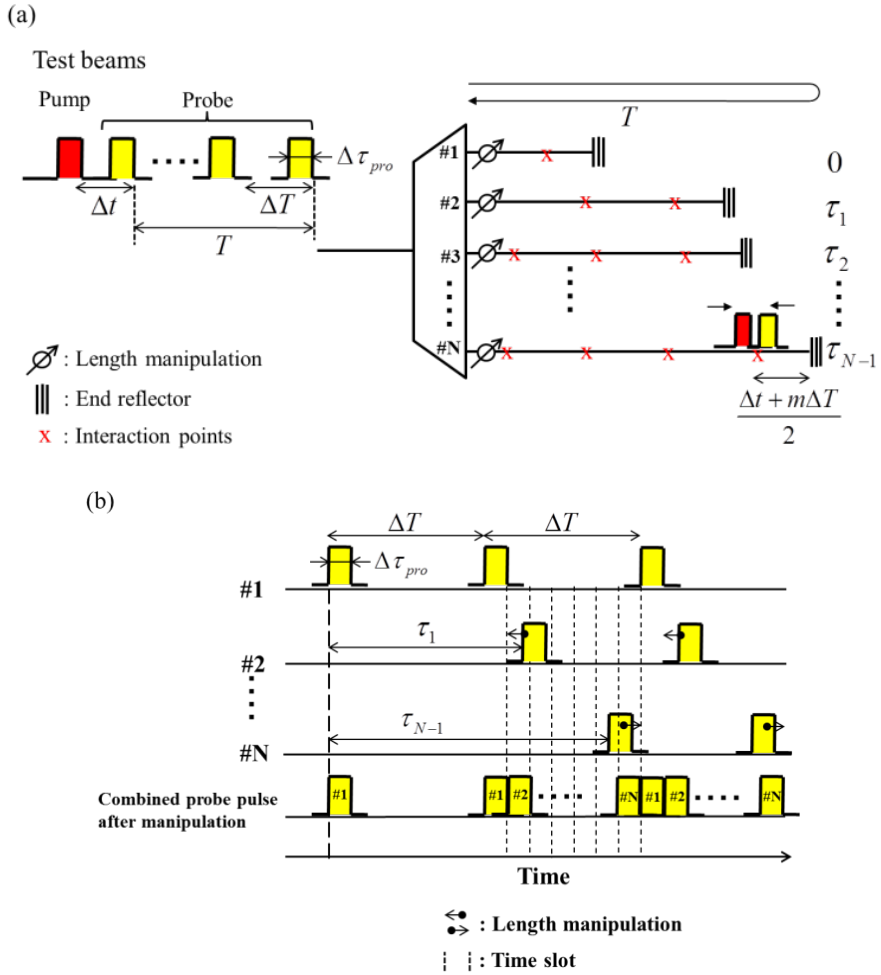

Fig. 3-2. (a) Proposed Brillouin analysis configuration for monitoring branched optical fiber. (b) Length manipulation technique for identifying probe pulses from each branched fiber.

3.3 Experiment

The experimental system, which is shown in Fig. 3-3, is similar to that described in [3-7] except for its use of the newly designed multi-probe pulse train. The probe and pump beams were intensity modulated with acousto-optic modulators (AOMs), with the electrical pulses programmed in the manner described in section II. The frequency of the probe beam was downshifted by the Brillouin frequency shift by using a single sideband modulator (SSBM) as a frequency shifter. By changing the sinusoidal frequency f_B input to the SSBM, the frequency of the probe beam was swept to observe the Brillouin gain profiles at each point.

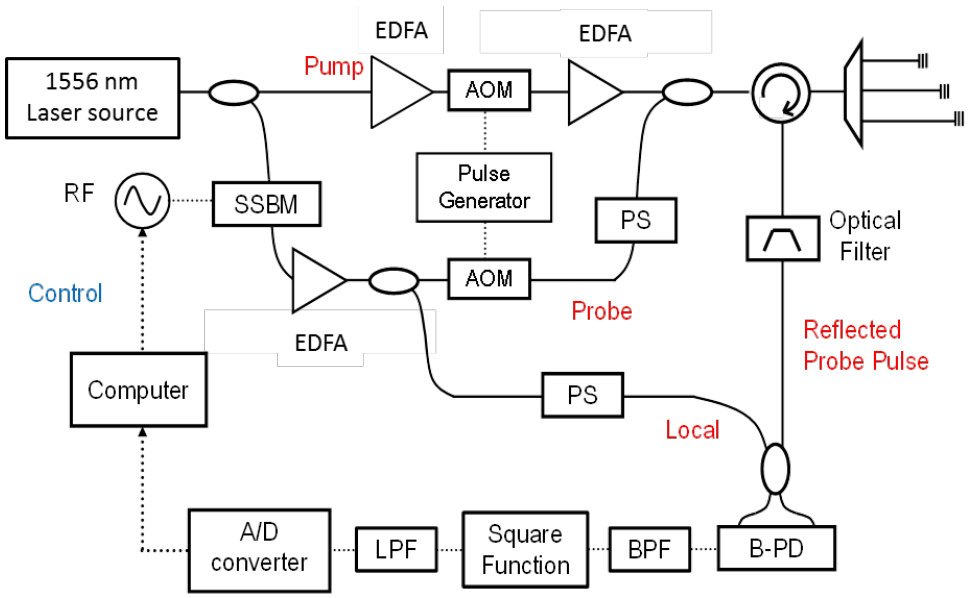

Fig. 3-3. Experimental setup for end-reflection assisted Brillouin gain analysis, SSBM: Single side-band modulator, AOM: Acousto-optic modulator, EDFA: Erbium doped fiber amplifier, PS: Polarization scrambler, B-PD: Balanced photo-detector, BPF: Bandpass filter, LPF: Low pass filter.

The branched fiber network used here is depicted in Fig. 3-4. The network included 4 branches. The fibers used for all the branches had a specified length of 1000 m (± 1 m). The length of each branch was manipulated by inserting 2 m-long patch cords behind the splitter. The lengths of the branches measured by OTDR (resolution: 1 m) were 1000, 1004, 1008, and 1012 m, respectively, or in terms of delay time, there were roundtrip delay differences of 40 ns ($\Delta\tau_{pro}$) between every neighboring pair, hence, the probe pulse interval, ΔT, was designed to be 160 ns. The entire roundtrip time, T, was about 10 μs, so that the ideal $T/\Delta T$ is ~62. To investigate the ability to detect temperature change, part of a specific branch (#2) was immersed in a temperature-controlled hot bath.

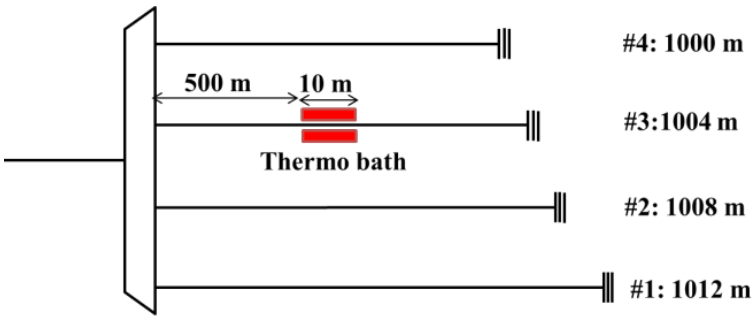

Fig. 3-4. Configuration of branched fiber network.

The test beam design is described in detail below. The probe and pump beams were emitted from the same semiconductor laser oscillating at 1556 nm. The probe and pump beams were carved by an acousto-optic modulator to generate 40 ($\sim T/\Delta T$) sequential probe pulses with a width of $\Delta\tau_{pro}$ = 40 ns accompanied by a single 40 ns wide pump pulse. The actual probe pulse repetition period, ΔT, was set at 333 ns, while the strictest design can reduce ΔT to $N\Delta\tau_{pro}$ = 160 ns. By scanning the time interval Δt from 0 to 333 ns, the analysis was accomplished for the entire range. By scanning the frequency shift of the probe beam, Brillouin spectra were obtained over a 160 MHz range. The incremental step of the optical frequency and the time interval were 2 MHz and 14 ns, respectively. The measurement was repeated 5000 times for a specific probe optical frequency and pump time delay to average the Brillouin gain. The peak Brillouin frequency shift at each interaction point was determined by quadratic fitting.

Fig. 3-5 shows the Brillouin spectra obtained around the hot bath in the heated branch. Spectra obtained in other branches are also shown for comparison. The variation in the Brillouin spectra around the heated point was clearly shown. In this case, the spatial resolution was determined by the pump pulse width (40 ns) at about 4 m.

Fig. 3-6 shows the dependence of the Brillouin frequency shift observed at the hot point at the target temperature of the hot bath. It was seen that the proportional coefficient is 0.93 MHz/°C, which agreed well with the commonly accepted value for silica glasses.

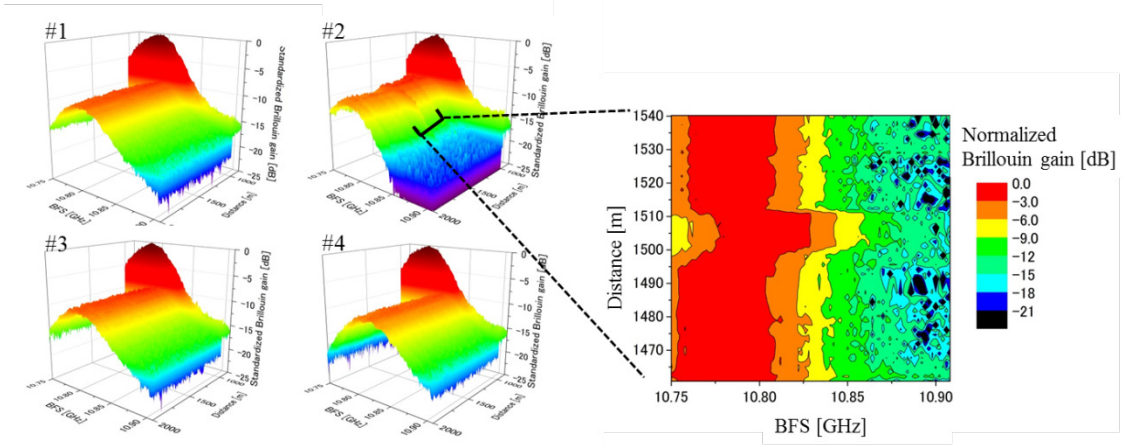

Fig. 3-5. Measured Brillouin gain spectra distribution in branched fiber. The part of the fiber around the heat bath in #2 is shown as an enlarged figure.

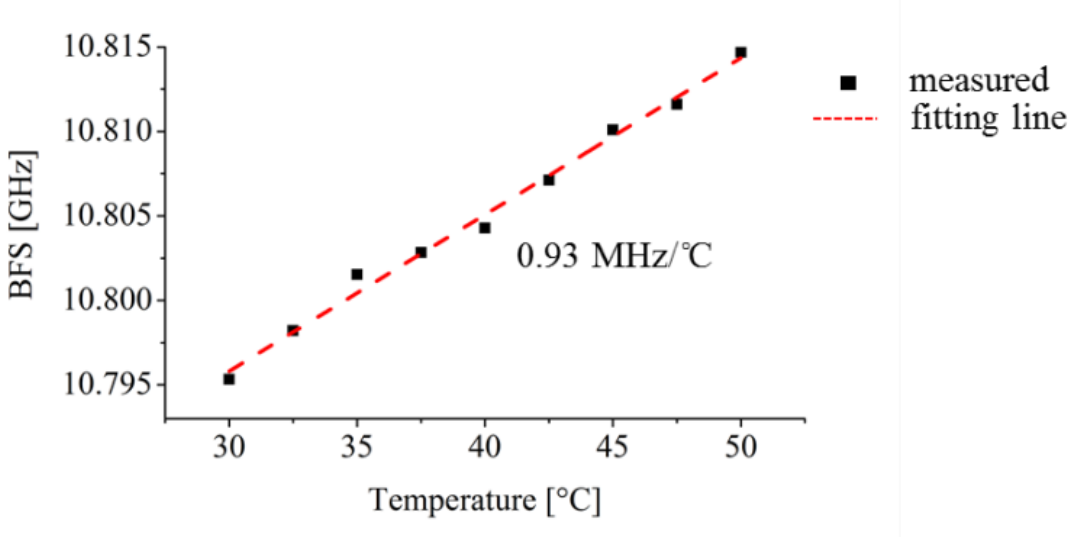

Fig. 3-6. Temperature dependence of Brillouin frequency shift measured at hot bath point of branched fiber #2.

To confirm the BFS error of the above experiment, Fig. 3-7 shows the BFS error distribution after fitting by using quadratic fitting in branched fiber #1. To analyze the BFS error, the standard deviation of the BFS distribution was calculated from a set of 30 close positions. The strained region caused by bobbin winding between 700 m and 1000 m was omitted from the evaluation. The average calculated error was 0.64 MHz and it was distributed evenly in the longitudinal direction. The sensing accuracy was almost same as the recently reported value for standard BOTDA [3-9].

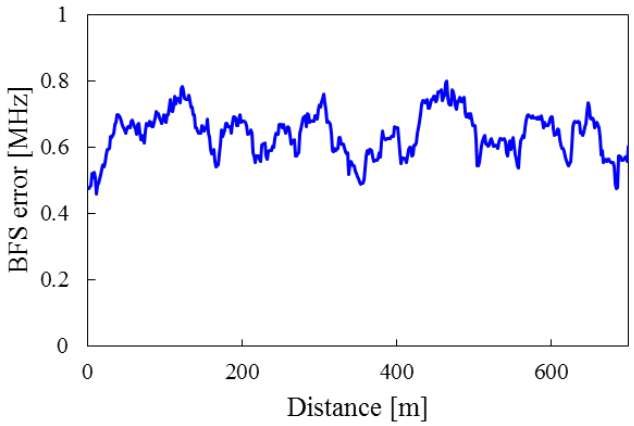

Fig. 3-7. Error of Brillouin frequency shift after quadratic fitting for branched fiber #1.

3.4 Discussion

The branch sensing topology provides a highly robust sensing network by comparison with conventional BOTDA with a unicursal topology where the entire system can easily shut down the result of a single fault on a sensing fiber. In addition, the proposed branch sensing system has the merit of flexible scalability on demand. In this section, author compares the proposed branched system and conventional BOTDA with a single unicursal fiber in terms of detection sensitivity with the same available input optical power.

Fig. 3-8 shows the two sensing systems compared here. In the proposed branched system, the number of branches, branched fiber length and branch length difference are set at N, L and $\Delta L/2$, respectively, while conventional BOTDA uses a single fiber whose length is NL. Accordingly, the total sensing length is NL in both systems. The pulse widths of the pump and probe beams in the proposed system are set at $\Delta L/v_g$, where v_g is the group velocity of the light in the fiber. The conventional BOTDA uses a pump pulse width of $\Delta L/v_g$ and a continuous probe beam. As a result, the spatial resolutions of both systems become ΔL. The available pump power for both systems is +15 dBm at the fiber input (before the splitter in the case of ERA-BA). The probe power is selected appropriately so that the SNR is maximized at the fiber far end in both systems. This is described later. With the conditions described above, the signal-to-noise ratios (SNRs) of the two techniques were compared as a sensing performance indicator.

First, note that the time needed to perform a single measurement over the entire fiber length is almost the same in both systems. Obviously, the single measurement time in the BOTDA is NL/v_g. The time is also NL/v_g in the proposed system, because it

requires N scans of Δt, while it accomplishes N simultaneous measurements in N branches. Therefore, when comparing the two systems, the SNR of the single measurement directly reflects the SNR obtained in the same measurement time. If author assumes that the optical receiver noise is the same in both systems, the comparison results in the magnitude of the obtained Brillouin gains in the systems.

Here, author analyze the Brillouin gain obtained at the far end of the sensing fibers (the worst SNR points) in the two systems. In both cases, the Brillouin interaction in the fiber is governed by the coupling equations below:

$$\frac{dP_p}{dz} = -\frac{g_B}{A_{eff}} P_s P_p - \alpha P_p \tag{3-1}$$

$$-\frac{dP_s}{dz} = \frac{g_B}{A_{eff}} P_p P_s - \alpha P_s \tag{3-2}$$

where P_p and P_s are the pump and probe powers at the interaction point, z is the distance along the fiber, g_B is the Brillouin gain coefficient, A_{eff} is the effective area of the fiber core, and α is the fiber loss coefficient. By numerically solving the equation, including the branch loss for the proposed system, the pump intensities when it interacts with the probe beam at the far end can be found. The parameters used in the simulation are as follows: g_B: 5×10^{-11} m/W, A_{eff}: 5×10^{-11} m^2, and α: 4.6×10^{-5} /m.

If the input probe power is increased, the increased detection power improves the SNR, while on the other hand, the increased pump depletion effect degrades it. To solve the problem of the trade-off, author numerically simulates the coupling equations for several probe beam powers and find the pump power when it interacts with the probe beam at the far end, and then analyze the obtained signal amplitude caused by the Brillouin gain. The probe power increment, $\Delta P_s(L)$, for the proposed branch sensing and $\Delta P_s(NL)$ for the BOTDA, can be given as follows;

$$\Delta P_s(L) = \frac{g_B}{NA_{eff}} P_s(L) P_p(L) \Delta L \exp(-\alpha L) \qquad \text{for ERA-BOTDA,} \qquad (3\text{-}3),$$

$$\Delta P_s(NL) = \frac{g_B}{A_{eff}} P_s(0) P_p(NL) \Delta L \exp(-\alpha NL) \qquad \text{for BOTDA.} \qquad (3\text{-}4)$$

Here P_p(z) and P_s(z) stand for the pump and probe powers, which can be calculated numerically by solving Eq. 3-1 and Eq. 3-2 , respectively.

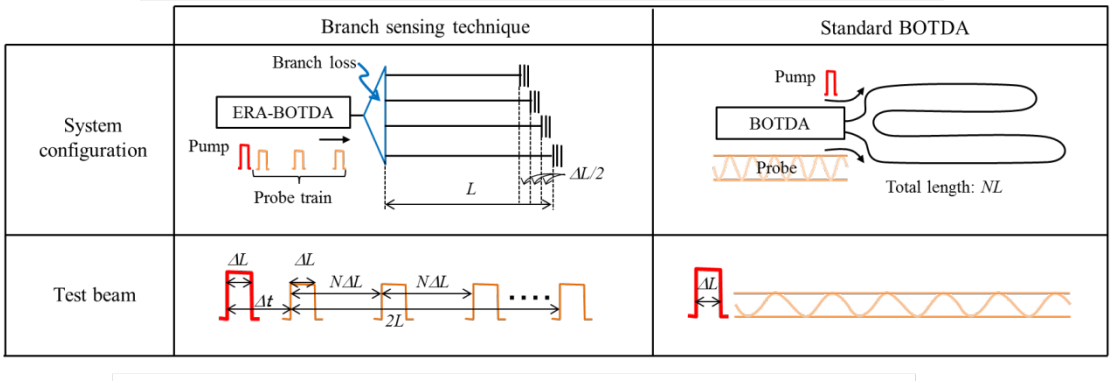

Fig. 3-8. The conditions for the system comparison. The sensitivity enhancement caused by the averaging effect is negligible in this comparison because the times required for monitoring the entire network are the same.

Examples of the results obtained for the proposed system and conventional BOTDA are shown in Fig. 3-9(a) and (b), respectively. Here, the increments of the probe power at the far end are calculated as a function of the input probe power, and normalized with respect to the maximum values for each total distance. The simulation results show that there are optimum probe powers for maximizing the signal amplitudes that consequently maximize the SNRs in both systems. By using the optimum probe power, author calculated the signal amplitudes at the far end of the fibers with a constant input pump power of +15 dBm.

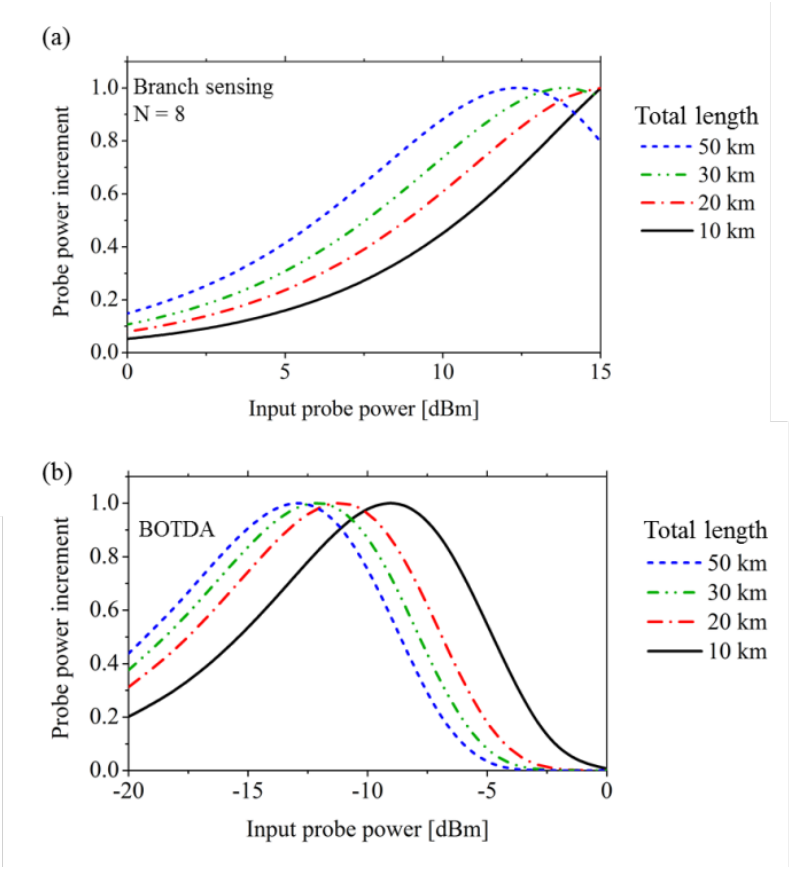

Fig. 3-9. Simulation results of the optimum probe powers for maximizing the signal amplitudes at the far end, of (a) the proposed technique for 8-baranch sensing and (b) BOTDA.

Fig. 3-10 shows examples of the probe power increments when the total sensing lengths are 60 km for both systems. As seen in the figure, the distributions of the probe power increment are flattened by using large numbers of branches. This is because there is accumulated pump depletion in BOTDA, while the proposed branched system suffers from less pump depletion. Moreover, even at z=0, the branched system yields larger signal amplitudes. This is because we can use a stronger probe in the branched system, while in conventional BOTDA, the probe power should be suppressed to avoid the pump depletion to reach the far end. Here author focused on the minimum probe power increment in the sensing areas to ensure the worst SNR values for the entire system. The minimum increment values are given at the far ends of the fibers from the pump input ends, and are $z=L$ for the proposed branch sensing and $z=NL$ for BOTDA. It can be seen that, the minimum probe increments with the proposed branch sensing can be larger than those with BOTDA even though the pump powers in the proposed systems are significantly attenuated by the splitter loss.

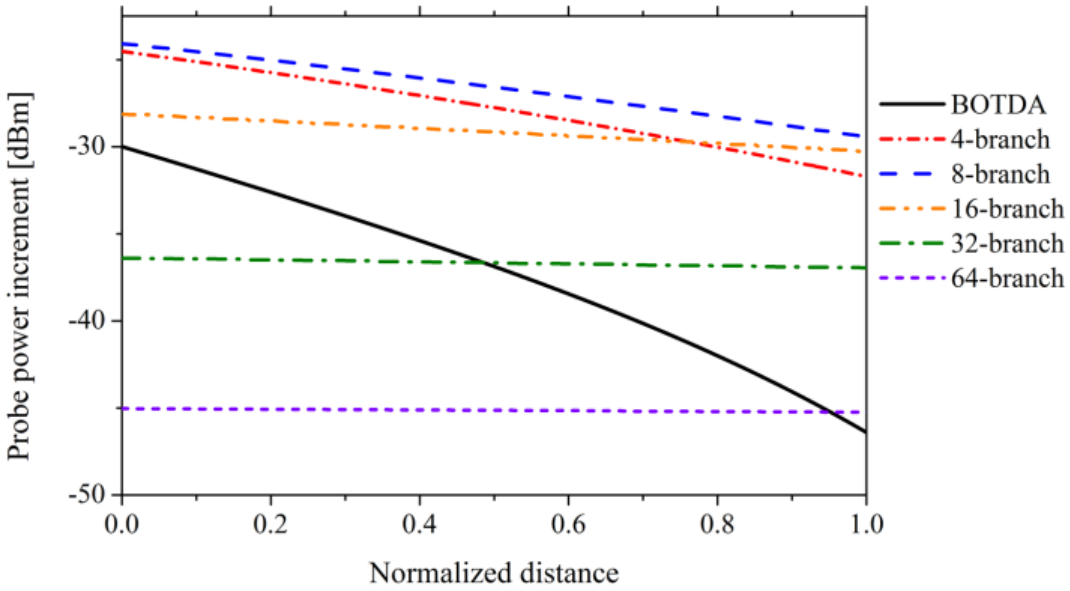

Fig. 3-10. Example of simulated probe power increment (Brillouin gain) distributions for the proposed branch sensing (break lines) and the BOTDA (solid line). The total sensing lengths are 60 km. The horizontal axis shows the distance normalized by L (for the proposed branch sensing) and NL (for the BOTDA).

Fig. 3-11 shows simulated and experimental results for the figure of merit (FOM) of the proposed system (the relative probe power increment at the far end) with respect to conventional BOTDA, as a function of branch number. The simulation result is the ratio of Eq. 3-3 and Eq. 3-4. Various total sensing lengths from 5 km to 60 km are simulated. For the experimental result, the ratio of the Brillouin gain between the two systems is plotted as the FOM. Author found that the experimental results agree with the simulations for total sensing lengths of 40 and 60 km. Here it should be stressed that, for a wide range of the total lengths, the proposed system can outperform the conventional BOTDA if author chooses the branch number appropriately. In addition, the FOM has its peak value, so the number of branches should be chosen to maximize the system performance. For example, an improvement of about 17 dB is achieved for a total fiber length of 60 km, which seems to be very large. As described above, the improvement is mainly due to the fact that the branched distribution of the probe beam suppresses the pump depletion effect, and enables a large pump power to be used at the far end. It seems that the result is important since it reveals the useful performance of the proposed branched sensing technique for 2- or 3-dimentional sensed objects.

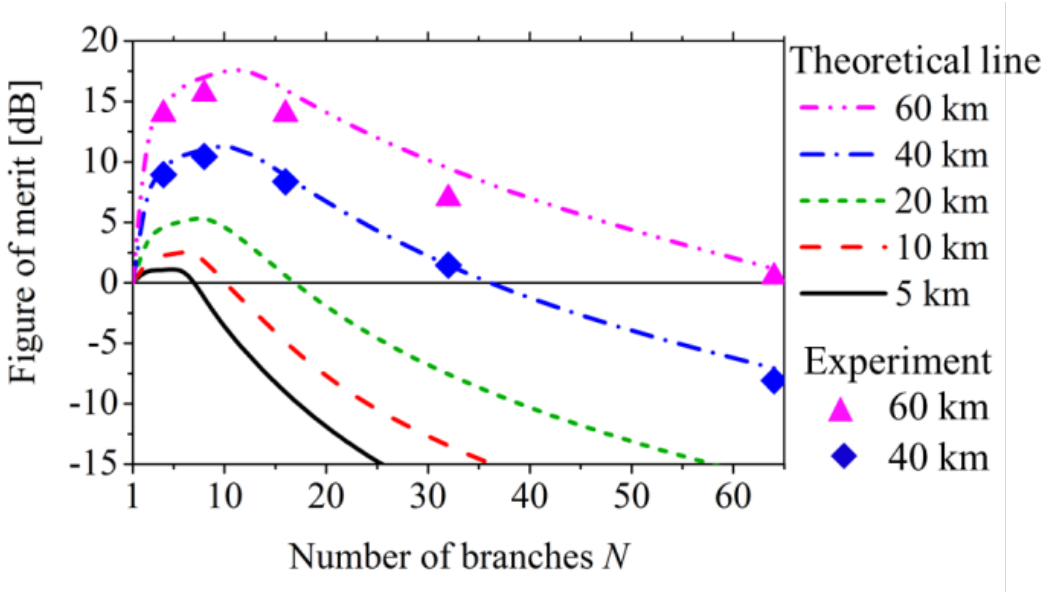

Fig. 3-11. Simulated and experimental results of the figure of merit of the proposed branch sensing for BOTDA with various total sensing lengths.

3.5 Conclusion

Author investigated a novel optical time domain Brillouin analysis technique, which includes branch sensor fibers that are connected by a passive power splitter, to enhance system reliability and flexibility, as well as the signal-to-noise ratio with respect to conventional BOTDA, which consists of a unicursal fiber topology. Author described a probe pulse arrangement designed to enhance the utility of the time sequence and so greatly reduce the measurement time. The technique is based on a previously proposed end-reflection assisted time-domain Brillouin analysis approach for monitoring branched fiber networks [3-6], [3-7], however, this chapter yields a novel (and author believe very important) finding, namely that the proposed system with a branch fiber network can outperform the conventional unicursal BOTDA in the signal to noise ratio, by choosing an appropriate number of branches. The simulation shows that, instead of branch loss, the avoidance of pump depletion in the branch configuration enhances the signal power at the far end of the fiber. Additionally, the branch topology increases reliability against sensing fiber faults. The branched topology would be especially useful when the sensed object occupies 2- or 3-dimensional space.

4 Applicability of end-reflection assisted Brillouin analysis in field

4.1 Introduction

The number of fiber to the home (FTTH) service users has been increasing rapidly and communication carriers are making an effort to reduce the maintenance costs incurred by massive amounts of optical equipment. To provide the FTTH service, a passive optical network (PON) is commonly employed in an optical access network, in which a passive power splitter is inserted between the customer's premises and the central office to reduce construction costs. A diagnostic issue remains in relation to the remote surveillance of PON branches. Traditional optical time domain reflectometry (OTDR) only provides a superimposed backscattering trace from all the branches, thus making it difficult to understand the fault position and loss value in a branch. As a result, the operator cannot completely ensure the health of the optical fiber without access to the customer side [4-1]-[4-3].

Recently, a novel technique was proposed for loss measurement in PONs called "end-reflection assisted Brillouin analysis (ERA-BA)," which distinguishes individual branches by using end-reflections at the terminated ends and their different branch lengths [4-4]. With this technique, loss information about individual branches is obtained by analyzing the local Brillouin gain at the position where the collision occurs between a pump pulse and probe pulses reflected from the ends of the branched fibers. Previous report has already measured a 32-branched PON in the laboratory [4-5].

However, the performance in the field has not yet been demonstrated. In principle, the statistical properties of the fibers deployed in PONs are the keys to designing the technique. The first property is the length of the branched fibers, which impose requirements on the measurement in terms of branch discrimination capability and spatial resolution. Another property is the Brillouin frequency shift (BFS) variation along installed fibers, which is caused by manufacturing, construction and environmental factors. It is important to investigate these statistical properties for practical applications since optical fibers have not intentionally been deployed in the field from the viewpoint of Brillouin characteristics.

In this chapter, author describes a technique for measuring the loss distribution of PON branches by employing ERA-BA in the field. The proposed technique employs the frequency shift averaging (FSAV) approach to compensate for the BFS variation in the field. Author also acquires the statistical distribution of branch length and BFS variation in deployed PONs, which is useful when considering the required specifications for practical use.

In actual PON systems, the branches are not limited to be terminated by a cut-off filter as mentioned in section 2. There are other possible fiber-end conditions such as an open connector end or a fractured end before services start or when damaged. Under these conditions, a broken fiber end or a fiber end cut with nippers reflects a probe pulse with a reflectance of ten or so decibels less than with a cut-off filter. The signal to noise ratio (SNR) of the measurement result by ERA-BA becomes worse when we use such a low reflectance fiber end. In this section, with the aim of applying ERA-BA to PON branch monitoring under any fiber end-face condition, author also clarify the potential of the method for use with the low end-reflection caused by a broken fiber end-face.

4.2 Issues when deploying ERA-BA in the field

4.2.1 Variation in Brillouin frequency shift in installed optical fibers

A BFS variation directly affects the loss measurement precision of ERA-BA in practical use. BFS variations are caused by the mechanical and environmental conditions of the installation or by climatic change, because the BFS is sensitive to strain and temperature [4-6], [4-7]. Figure 4-1 is a schematic illustration of possible factors causing BFS variations in the field. For example, as seen in Fig. 4-1, the temperatures differ in cable sections exposed to direct sunshine or in the shade, and also differ when the cables are installed underground, aerially, and in buildings. The residual strain applied to cabled fiber during manufacture and after construction is also a cause of BFS variation. In an earlier study [4-8], it was reported that a residual strain of less than 0.1% was distributed along cabled fiber after construction, which corresponds to a 50 MHz shift in the BFS. Figure 4-2 shows various BGSs of standardized fibers (ITU-T G.652.D [4-9] and G.657.A [4-10]), which are widely deployed in PONs. They exhibit at least a 100 MHz difference in BFS. The multiple deployments of different types of fiber and/or different manufactures are dominant factors affecting BFS variation. Therefore, a frequency range covering several hundred MHz should be compensated for in a field measurement.

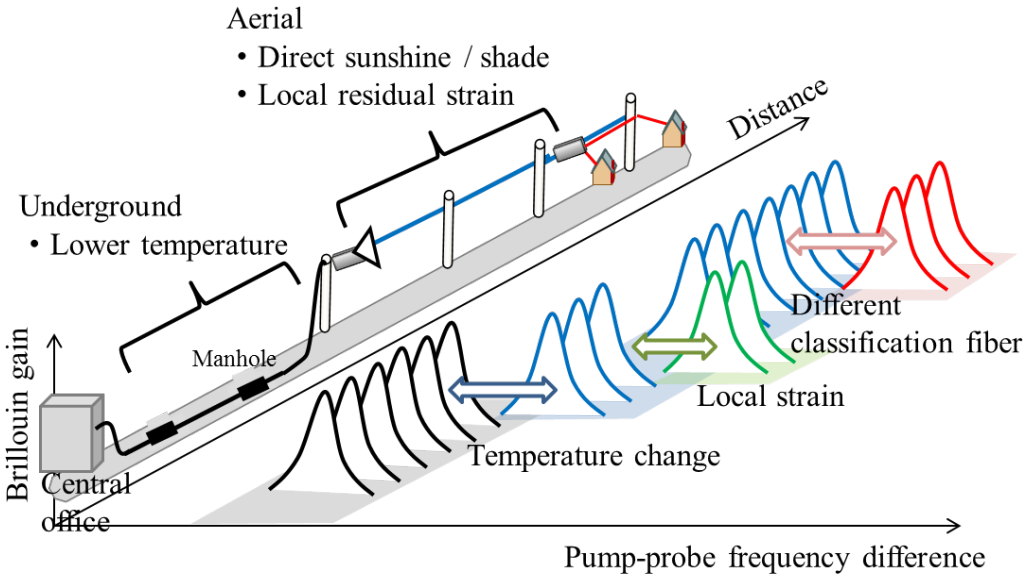

Fig.4-1 Primary factors behind BFS variations in practical PONs.

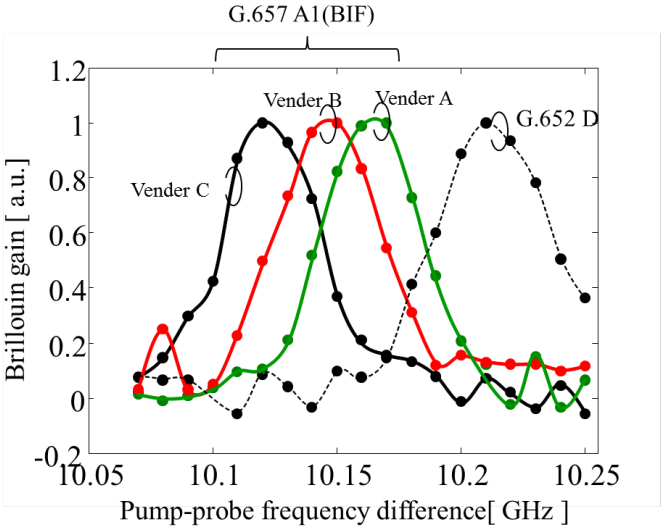

Fig.4-3 The various BGSs of different manufacturers' fibers and standardized classification.

4.2.2 Brillouin frequency shift averaging (FSAV)

A possible way to compensate for a range of BFSs in the field is the FSAV approach. In this approach, the Brillouin gain spectra (BGSs) in the expected frequency range along cabled fibers are obtained by changing the pump-probe frequency difference (Fig. 4-3 (a)). The following two methods can be considered for FSAV. One is called “peak search” and the other is called “spectral averaging.” The peak search method depicted in Fig. 4-3 (b) traces the peak gain of the obtained BGS. On the other hand, the spectral averaging method shown in Fig. 4-3 (c) calculates the average values of the Brillouin gain over the FSAV range obtained from the BGSs. The spectral averaging method in Fig. 4-3(c) results in handling smaller signal amplitudes (gains) than the peak search method.

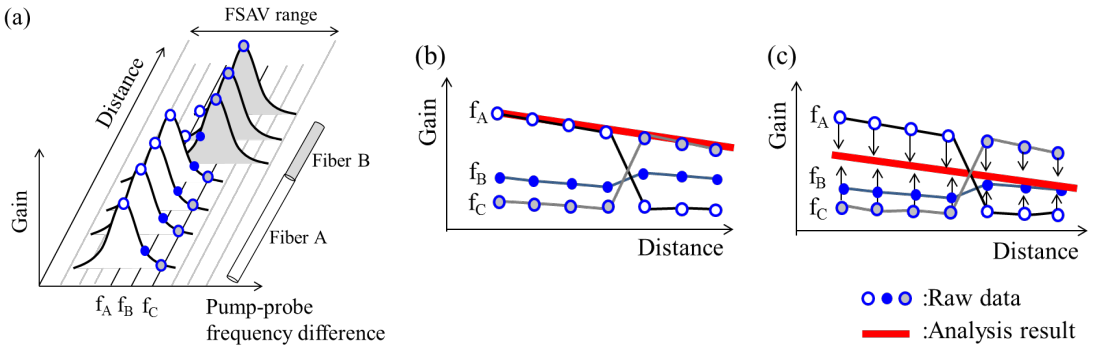

Fig.4-3 FSAV approaches for the proposed technique to compensate for BGS variation in a practical PON system. (a) Schematic FSAV image of Brillouin analysis, (b) peak search method, and (c) spectral averaging method.

4.2.3 ERA-BA for broken PON monitoring

In the deployed PONs, the branches are not always terminated by a cut-off filter. There are other possible fiber-end conditions such as an open connector end or a fractured end before services start or when damaged. Thus, the ERA-BA should be examined with low end-reflectance before its practical use. All the case for branch monitoring, including broken fiber, every length must be different; otherwise same length branches cannot be identified. In other words, the test probe pulse width should be smaller than the minimum optical path difference.

Here, author focus on the influence of end reflectance on the measurement result since the probe pulse is not always reflected by a cut-off filter, when considering a branch end before service starts or when there is a breakage. The end reflectance value has a direct influence on the SNR of a measurement result because of the decrease in the detected probe pulse power. The dynamic range of the proposed method has already been described [4-11]. Here, when taking account of the end reflectance R [dB], the single way dynamic range (SWDR) is given by

$$SWDR[dB] = \frac{1}{3}\left(R + P_{probe} + P_{pump} + \beta - P_d + 5\log(N)\right) \quad (4\text{-}1)$$

where P_{probe} [dBm] and P_{pump} [dBm] are the input peak powers of the probe and pump pulses, respectively. And is the Brillouin gain factor. P_d represents the minimum detectable power of the receiver. The last term describes the N times averaging effect. Thus, one-third of the decrease in the end reflectance contributes to a decrease in the dynamic range.

4.3 Pre-inquiries on installed PONs

4.3.1 Typical PON configuration in Japan

Figure 4-4 shows a typical access network configuration in Japan. With the passive double star topology, a 4-branched optical splitter is installed inside an office and an 8-branched splitter is installed in a distribution area near the customers' premises. A test coupler is employed for in-service optical measurement just below the 4-branched splitter. A fiber Bragg grating based test beam cut-off filter [4-12] is installed just before an optical termination unit (ONU) on the customers' premises. The filter allows the communication wavelength to pass and reflects only the maintenance wavelength with a high reflectivity, which can be used as an end reflector in the ERA-BA. The splitter is not cascaded for in-service testing from the test coupler, thus it can be considered that any differences in the round-trip time of reflected probes are given by the branch fiber lengths below the outside 8-branched splitter.

Figure 4-5 shows two types of network configuration that have been optimized for cost-effective construction in accordance with the amount of FTTH demand. As shown in Fig. 4-5(a), 8-branched splitters are installed in the center of the distribution blocks [4-13], and are used for high penetration areas such as urban areas. Only drop cable is used from the splitter at the distribution point to the customer's premises. On the other hand, in low penetration areas (Fig. 4-5 (b)), the splitters are installed at the front edges of the distribution blocks. Distribution cable is used from the splitter to the drop point at a telegraph pole near the customer's premises. It can be seen that the branch length tends to be longer than those in Fig. 4-5(a).

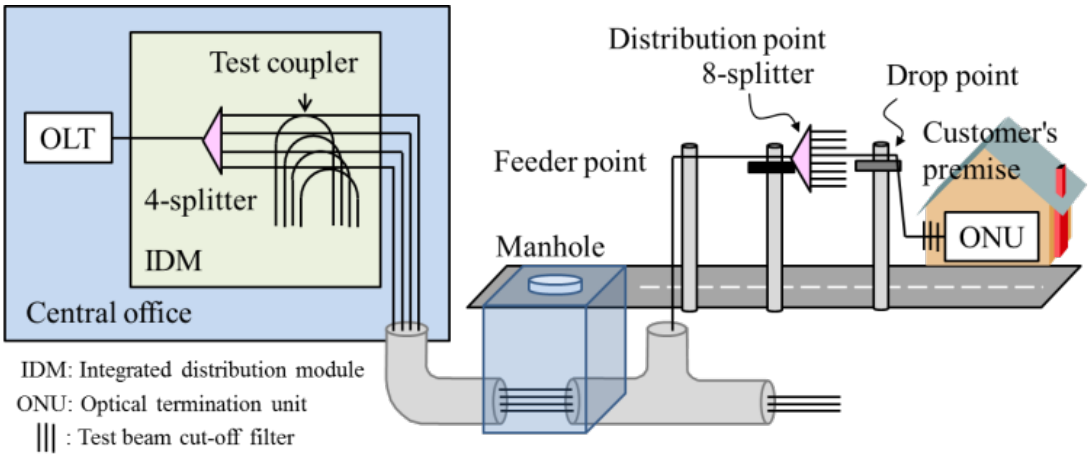

Fig.4-4 Typical access network configuration in Japan.

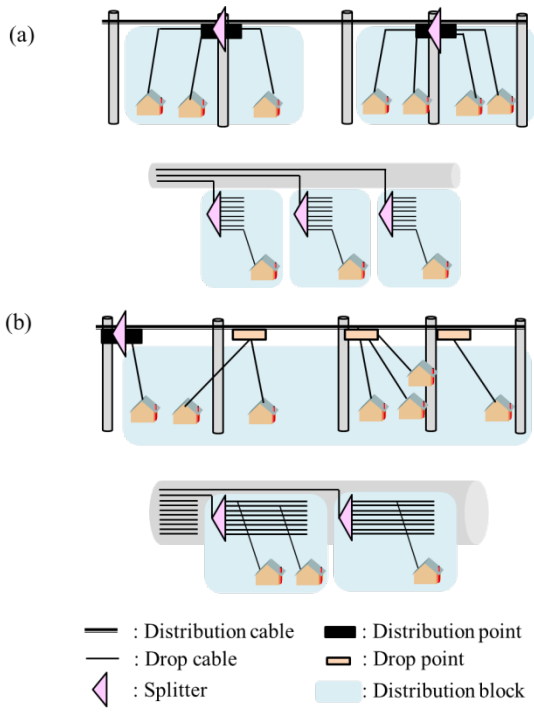

Fig.4-5 Two types of network distribution (a) splitter at drop point in center of distribution block, and (b) splitter at distribution point at the front edge of distribution block.

4.3.2 Branch length statistics in installed PONs

Author investigated the branch length and its length difference in field PONs providing services for detached houses in certain areas in Japan. The branch length was measured with OTDR, and obtained from the events of the splitter loss and the reflections at the cut-off filters in the OTDR trace. Author undertook the investigation from two central offices in urban and rural areas employing the network configurations shown in Fig. 4-5 (a) and (b), respectively. The spatial resolution of the OTDR was up to 30 cm.

Table 4-1 shows statistical properties of the branch length measured in the field. The branch length was widely distributed from several meters to over one kilometer. The shortest branch length was 2 m, and the mean branch lengths were hundreds of meters. Table 4-1 shows that a spatial resolution of better than 10 m is expected to be required to cover all installed PONs, while a spatial resolution of several tens of meters might be sufficient to identify more than about 90% of the branched fibers in installed PONs. Note that the pump pulse width should be designed to provide an appropriate spatial resolution since there is a trade-off between the pump pulse width and the signal-to-noise characteristics in ERA-BA [4-5], as well as other distributed measurements.

Table 4-2 shows the statistical properties of the branch length difference, which is given by the distance between two neighboring end-reflection events in the OTDR trace. The results showed that 99.8% of branched fibers can be detected by employing a probe pulse width of no less than 10 ns (i.e. a branch discrimination resolution of 1 m), which meets the theoretical limit for ERA-BA due to the acoustic rise time.

Table 4-1 Measured branch length results

Configuration		(a)	(b)
Number of samples		742	1366
Cumulative probability	-10m	1.6%	0.5%
	-20m	2.4%	1.1%
	-30m	5.5%	2.1%
	-50m	10.8%	5.1%
	-100m	28.6%	14.6%
	-200m	66.0%	38.4%
	-500m	90.8%	67.9%
	-1000m	98.4%	88.4%
Shortest branch length [m]		2.0	2.1
Mean branch length [m]		240	463

Table 4-2 Measured branch length difference results

Configuration		(a)	(b)
Number of samples		527	1048
Cumulative probability	-1 m	0.2%	0.1%
	-2 m	0.4%	0.7%
	-5 m	6.3%	3.2%
	-10 m	20.5%	12.3%
	-20 m	39.5%	26.1%
	-40 m	62.2%	48.1%
	-80 m	81.2%	67.7%
	-120 m	88.8%	78.1%
Shortest branch length [m]		1.0	0.5
Mean branch length [m]		58	95

4.3.3 Return loss of broken fiber edge

Author investigated the reflectance of a broken fiber end. Two damage event conditions were prepared, namely the fiber was broken by excess bending and cut by nippers. The reflectance was measured using optical continuous wave reflectometry (OCWR) [4-14]. The measurement was repeated 250 times for both conditions. Figure 4-6 shows histograms of the end reflectance of a broken fiber end caused by (a) excess bending and (b) cutting with nippers. According to these statistical distribution results, the majority of broken fiber ends to have a reflectance of -30 to -50 dB. This means that the applicability of the proposed method for monitoring the broken branch of a PON would be determined by whether or not the technique can cope with such low end reflectance.

4.3.4 Applicable range with low end reflectance

To clarify the potential of the proposed method, author simulated the measurement time for 8-branched model PON systems with various end reflectance values. The PON consisted of fiber with a total length of 2, 6, or 10 km including 1 km of branched fiber. Here, the optical fiber loss was set at 0.4 dB/km and the branching loss was 10.5 dB for an 8-branched splitter. And the measurement specifications were set at a fiber length identification resolution of 3 m and a fault location resolution of 15 m [4-5]. The probe and pump pulse powers were 13 and 16 dBm, respectively.

Figure 4-7 shows a simulation result. In a measurement time of 300 seconds, the proposed technique could cope with end reflectance values of up to -53, -46, and -40 dB, for 2, 6, and 10 km long fibers under test (FUT), respectively. According to Eq. 4-7, if the PON has larger loss than simulation assumption, the allowable reflectance proportionally deteriorates 3 dB when fiber loss increases 1 dB. For example, simulated 2 km fiber having 5 dB additional loss can be coped with -38 dB end reflectance (deteriorated from -53 dB).

The investigation of broken fiber end reflectance and the simulation result show that the proposed method could be used to monitor broken branches in a typical PON system with a distance of several km, using a low power retuned probe pulse yielded by a broken fiber end.

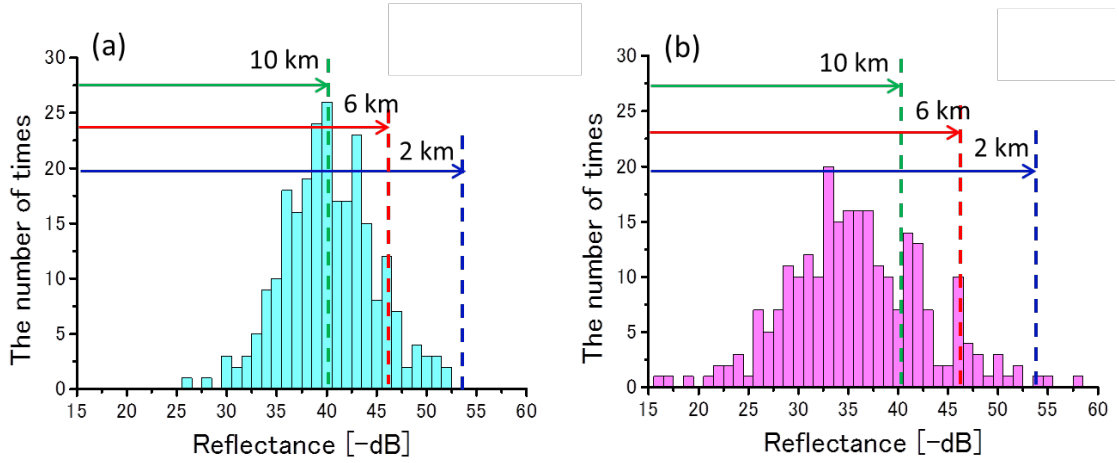

Fig. 4-6. Histograms of reflectance of broken fiber end (a) and cutting end (b), and measurable range in 300 seconds (Corresponds to Fig. 3).

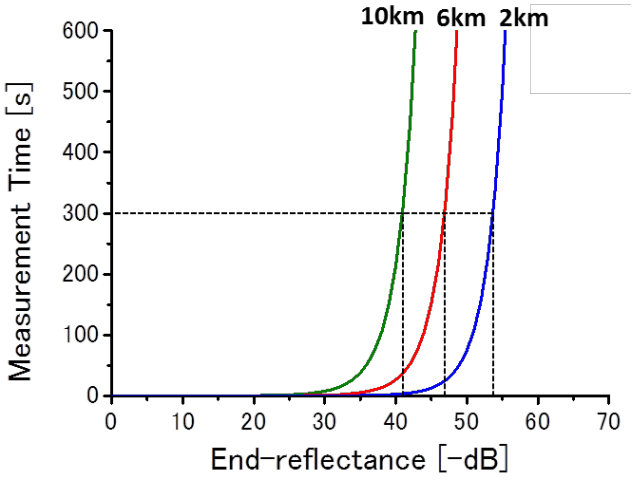

Fig. 4-7. Simulation result of measurement time with proposed method for various end reflectance values.

4.4 Field test and experimental demonstration

4.4.1 Equipment setup

Figure 4-8 shows the measurement system prepared for the field demonstration. The measurement system was based on that described in chapter 2. Two distributed feedback lasers were used to launch pump and probe beams in the 1650 nm maintenance band. The launched power levels of the pump and probe pulses were 22 and 9 dBm, and the pulse widths were 500 and 50 ns, respectively. Those pulse widths corresponded to a 50 m spatial resolution and a 5 m branch discrimination resolution. Both beam frequencies were controllable with an automatic temperature controller (ATC), an automatic frequency controller (AFC) and a Fabry-Pérot etalon filter as a wavelength locker. The ATC and AFC were used to control the frequency difference between two DFB-LDs with feedback current from a wavelength locker. The system performance consisted of a frequency precision of 1 MHz over a ±2 GHz bandwidth. The probe frequency was designed to change in 5 MHz steps. The total measurement time for one PON was about 30 minutes including time averaging and FSAV. A polarization scrambler, whose scrambling rate was sufficiently smaller than the measurement repetition rate, was used to exclude the effect of the polarization dependent gain on the results after the averaging process. Author examined 38 PONs providing services to detached houses. Each PON had the configuration described in section III. The pump and probe pulses from the measurement system were launched into the feeder fiber via the test coupler. The coupler typically had a 7 dB insertion loss for a 1650 nm maintenance band test beam [4-15]. The cut-off filters acted as probe pulse reflectors with a return loss of less than 1 dB in the maintenance band.

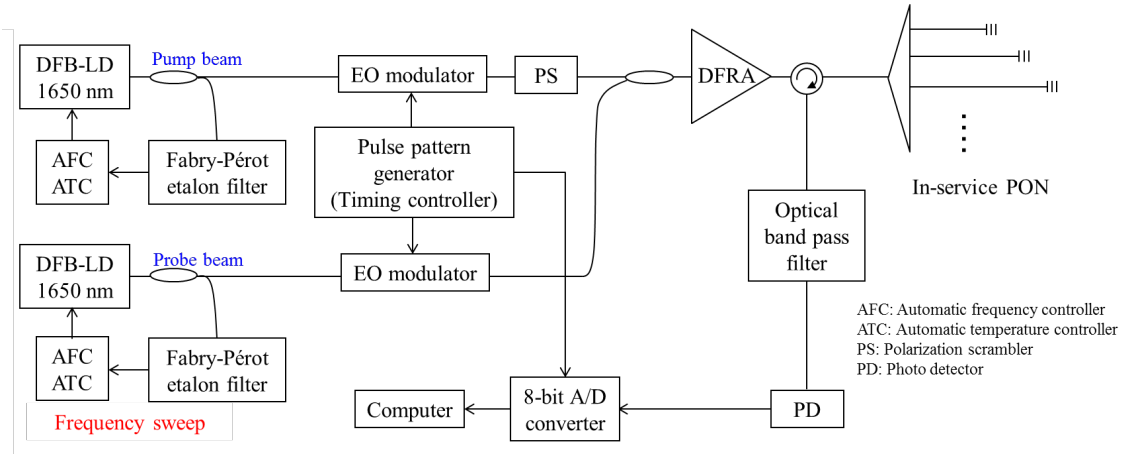

Fig.4-8 Measurement system for a field test employing a frequency shift averaging method to compensate for the BGS variation in an installed PON.

4.4.2 BFS variation measurement of deployed PONs

Figure 4-9 shows a histogram of the BFS in 38 deployed PONs obtained by analyzing measured BGS distributions with a spatial resolution of 50 m. The BFS was calculated by performing quadratic fitting over the full width at half maximum of the BGS. The BFS was varied over a bandwidth of about 210 MHz. The frequency sweep bandwidth was set of 300 MHz for the FSAV taking account of the additional bandwidth that was expected due to changes in climate, other temperature conditions (several tens MHz), and the Brillouin gain bandwidth (about 60 MHz).

Figure 4-10 shows some of the measured BGSs. The horizontal axes indicate the difference between the pump (f_{pump}) and probe (f_{probe}) frequencies. In Fig. 4-10(a), the 3 dB Brillouin gain bandwidth was about 60 MHz, which was slightly wider than the general value. Author believes this to be due to the effect of the residual strain distribution in the field within the spatial resolution. A BGS usually has one peak on a Lorentzian-like curve as shown in Fig. 4-10 (a), while some BGSs with double peak were also observed as shown in Fig. 4-10 (b). In general, a double peak BGS has a lower peak value and a wider bandwidth than a single peak BGS. With the peak search method, only a faulty result with apparent loss can be obtained in a section of the double peak BGS fiber. Since telecommunication fibers are not standardized in terms of refractive index and BGS, Fig. 4-10 implies that the spectral averaging method is much more suitable for FSAV than the peak search method.

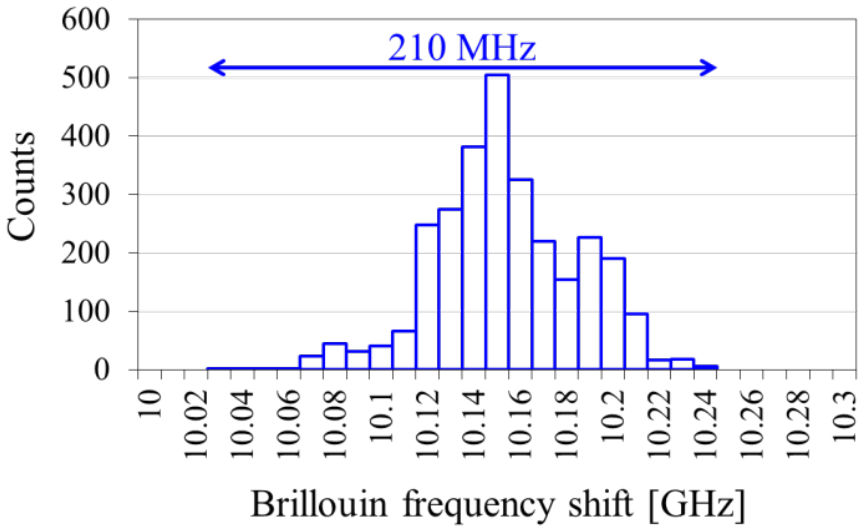

Fig.4-9 Histogram of Brillouin frequency shift (BFS) in 38 PONs. The BFS was analyzed by 50 m steps in BGS distribution.

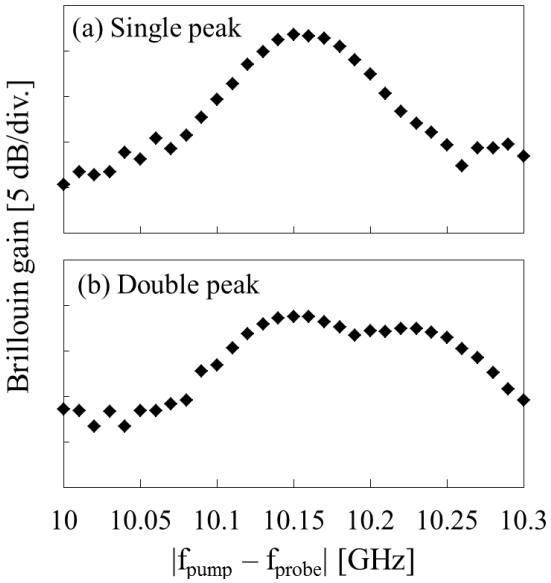

Fig.4-10 Obtained Brillouin gain spectra (BGSs). (a) Most parts of the fiber showed single peak in the BGS. (b) Some parts showed double peak.

4.4.3 Loss distribution measurement of deployed PON branches

Figure 4-11 shows demonstration results for loss distributions obtained with the spectral averaging method. The solid and broken lines in Figs. 4-11 (a) and (b) show the loss distributions with and without FSAV, respectively. The results without FSAV were obtained using a single pump-probe frequency difference of 10.15 GHz, which was the most frequent BFS in Fig. 4-9. The results clearly show that the spectral averaging method for FSAV is crucial in the field measurement, and that the branched fibers are successfully measured. The results show branched fibers with no faults over 650 m (#1) and 720 m (#2) and 8-branched splitters 5 km from the central office. The measurement accuracy with FSAV was still insufficient at ±0.25 dB. That was not the theoretical limit, but was dominated by the electrical noise of receiver system (cf. a photo-detector or 8-bit A/D converter) on pulse peak power. The future work will be to optimize the receiver system by redesigning the detected power level and to reduce the quantization noise.

It is noted that the splitter losses in Fig. 4-11 appear to be slightly smaller than the practical value. This is caused by a fiber property mismatch (e.g. mode field diameter and/or refractive index profile) between the feeder and branched fibers. Even though the BFS difference can be compensated for over the fibers, apparent gain or loss caused by the mismatches remains in the results as well in single-ended OTDR measurements. A quasi-bidirectional scheme for the ERA-BA is proposed in [4-16] for evaluating the loss accurately. Nevertheless, the results revealed the feasibility of using the approach for remote surveillance from a central office.

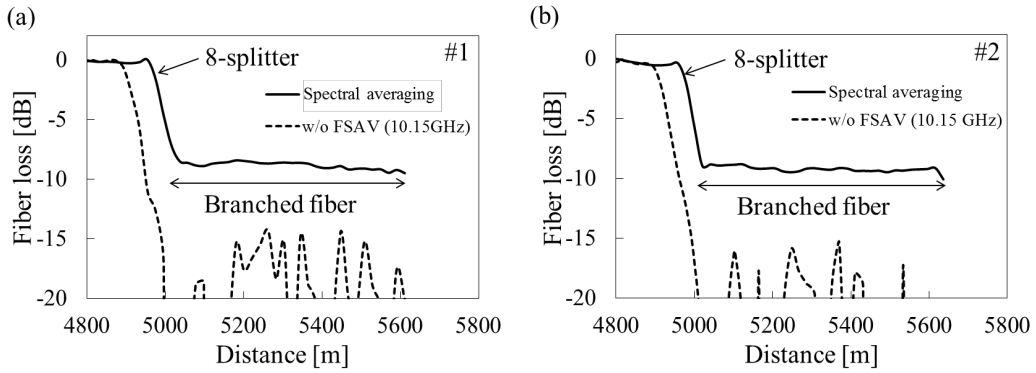

Fig. 4-11 Demonstration results of two-branch monitoring over an 8-splitter in the field. The spatial resolution was 50 m.

4.5 Demonstration of broken fiber monitoring in PON

Author demonstrated broken PON monitoring experimentally. Figure 4-12 shows the PON configuration monitored with the proposed method. It included an 8-branched optical splitter. Six optical fibers were attached to the output ports of the splitter. The other two ports were open. One of the branched fibers was terminated by a -40 dB reflection, which simulated a typical broken optical fiber. The remaining branches were terminated by an almost 100% reflector, which simulated healthy fibers. Additionally, badly connected super physical contact (SPC) polished connectors were installed in two branches, which yielded an impermissible reflection of from -30 to -40 dB, which could be mistaken for a broken end reflection. Figure 4-12 (b) shows a reflection trace of the measured PON. The observed reflection peak of (1) shows a small end reflection from the broken fiber end. (2)-(6) show end reflections from the cut-off filters. (7) and (8) show reflections at bad connections. Although the two open output ports of the 8-branched splitter also reflected the probe power, the measurement system can ignore it since the arrival time at the detector was sufficiently different from reflections (1)-(8) from the branches.

Both the pump and probe beams were generated from a laser diode at wavelength of 1556 nm. The frequency of the probe beam was downshifted by 10.80 GHz, which corresponds to the Brillouin frequency shift of single mode fiber, by using a single sideband modulator. Both beams were intensity-modulated by acousto-optic modulators with 250 MHz frequency shift. A probe pulse width was 30 ns and a pump pulse width was 150 ns. These pulse widths corresponded to a fiber length identification resolution of 3 m, and an event location resolution of 15 m, respectively.

The powers of the test pulses were 13 dBm for the probe pulse and 16 dBm for the pump pulse. The measured probe power was averaged 30000 times in 300 seconds. During averaging, probe beam and local beam polarization were scrambled by polarization scramblers to remove the polarization independency of Brillouin gain factor and heterodyne detection efficiency.

The power of the reflected probe pulse was observed by heterodyne detection. The beat signal at the frequency of 250 MHz was detected by balanced optical photo-detector. Here, the minimum detectable power was assumed about -82 dBm. The measured beat signal was converted to a baseband signal by envelope detection. The baseband signal was converted to a digital signal by using a 200 MS/s A/D converter. Under the above measurement conditions, a 10.3 dB SNR was theoretically expected for the loss distribution of the broken fiber.

Figure 4-13 shows the loss distribution measured by using the reflections (1)-(6). The loss distribution of the broken fiber was successfully measured in (a) with a 9.1 dB SNR, which agrees well with the theoretical value of 10.3 dB. Figure 4-13(b)-(f) show the loss distributions of healthy fibers.

Note that the reflections (7) and (8) may be also mistaken for broken ends, and the measurement system may analyze loss distributions by using these reflections. However, these misoperations can be avoided by carefully observing the loss distributions of healthy fibers. Namely, in Fig. 4-13(f) and (b), clearly see the loss events at distances of 551 and 769 m, which correspond to the positions of the returned probe pulses shown in Fig. 4-12(b)-(7) and -(8). Therefore, these loss events can be identified as bad connection losses. Here, the unneeded reflections caused at bad connections can be excluded by mapping the loss event location and time diagram of

reflections from the measured PON. Note that above identification scheme premise the state that the reflection from broken end does not arrive with other reflections just at the same time. In conclusion, the proposed method can fully monitor a practical PON configuration even with the typical low end reflectance assumed to be from a broken fiber end.

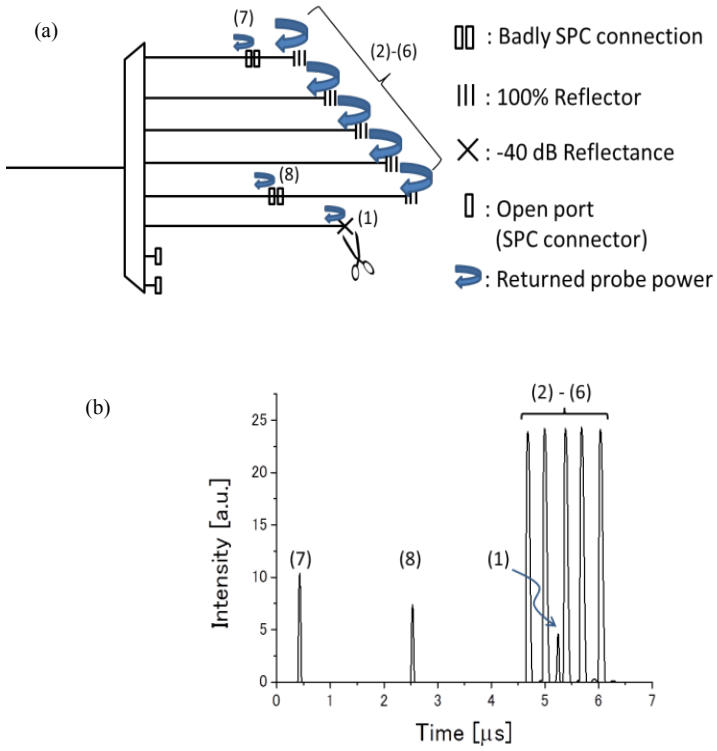

Fig. 4-12. (a) Configuration of PON including -40 dB reflectance end and two bad connections. The number in parenthesis corresponds to the reflection number in figure 5. (b) Reflection trace of returned probe pulse from 6 branches of FUT including -40 dB reflectance end and two bad connections.

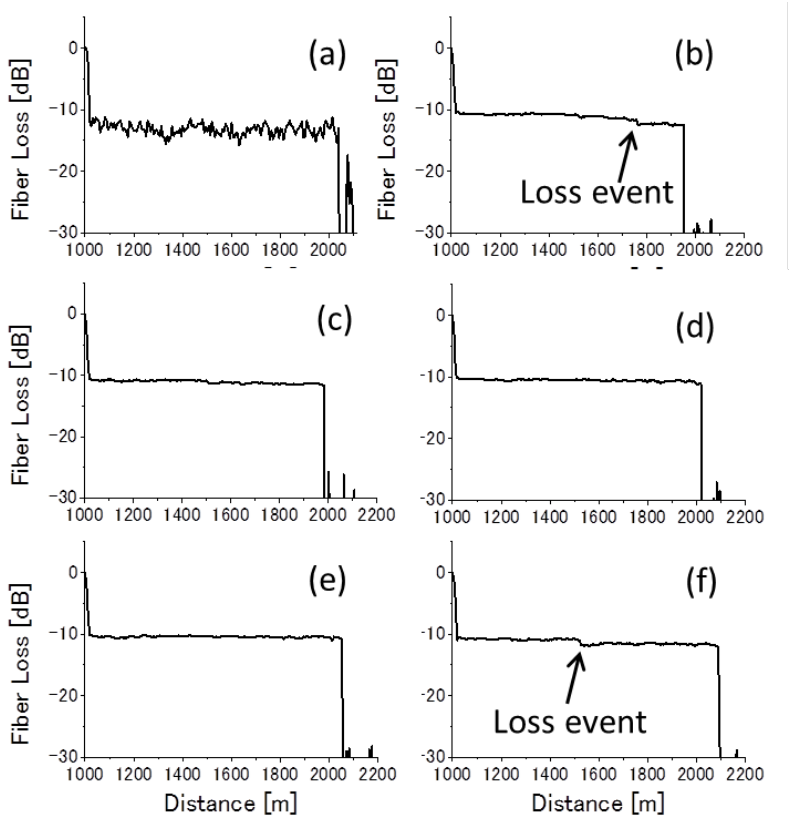

Fig. 4-13. Results of individual loss distribution measurements for PON.

4.6 Conclusion

Author demonstrated PON branch measurement by using ERA-BA in the field for the first time. The proposed FSAV approach successfully compensated for the field variation in the BFS, which ranged over several hundred MHz in deployed PONs. The result indicates that the proposed technique has the potential for practical use in reducing the operating expenses involved in centralized PON monitoring.

Author described broken PON monitoring by using end-reflection assisted Brillouin analysis. Author showed that the ERA-BA was applicable to typical PON systems even if some branches are not terminated or broken thus having low reflectance. The proposed method would be practical and useful for application to the maintenance of PONs since the technique can monitor PON configuration completely.

5 BOTDA with frequency-swept pulse for vibration measurement and simplified setup

5.1 Introduction

A large number of optical fiber sensing techniques have been studied with the aim of monitoring the distortion of social infrastructure. Brillouin-based sensing techniques such as Brillouin optical time domain analysis (BOTDA) [5-1] and Brillouin optical correlation domain analysis (BOCDA) [5-2] can measure changes in strain and temperature with high sensitivity by monitoring the Brillouin frequency shift (BFS). Fast BFS acquisition has recently attracted a lot of attention with a view to performing dynamic strain measurements [5-3]-[5-9]. Bernini et al. first proposed dynamic strain measurement with stimulated Brillouin scattering [5-3]. The method operated with less sensitivity because it used the Brillouin gain slope. Slope-assisted BOTDA [5-4] has been improved at a 1 kHz effective sampling rate in a 46 m sensing range by eliminating test beam frequency sweeping [5-5]. By taking advantage of its high sensitivity, BOCDA achieved a 5 kilo-points/s sampling rate over a 200 m range with a single-shot measurement [5-6]. Bao et al. proposed the method that avoids pump-probe frequency sweeping by analyzing the polarization dependent Brillouin gain [5-7]. Moreover, Brillouin optical correlation domain reflectometry (BOCDR) was improved by eliminating complicated frequency analysis, which was replaced by electrical signal processing [5-8] or self-delayed heterodyne detection [5-9]. However, there are reasons why it is difficult to expand the sensing range with these approaches: slope-assisted

BOTDA exhibits low sensitivity due to the small Brillouin gain in the skirt region of the Brillouin gain spectrum (BGS), and with BOCDA multiple correlated peaks appear over a longer range. Other studies reported ranges of only several hundred meters. Increasing the sensing range while maintaining a high-speed sampling rate is important in terms of expanding the application of dynamic strain measurement. Additionally, monitoring the infrastructure cost can be reduced with a long-range measurement system that covers a number of measured objects around a central office in which the system is installed.

In this chapter, author proposes a novel Brillouin-based sensing method for long-range and high-speed dynamic strain measurement with random access that author call frequency-swept pulsed BOTDA. The method employs frequency swept pump and probe pulses. author observe the correlated Brillouin gain (CBG) of a received probe pulse. With the proposed method, the time shift of a CBG peak can be perceived as BFS changes, and so dynamic strain can be easily measured with an oscilloscope. The novel approach can acquire a Brillouin gain profile instantaneously during a one-shot test pulse collision without any averaging or frequency step scanning. author demonstrate experimentally a 10 kilo-points/s dynamic strain measurement in a 10 km sensing fiber by using a simple system set-up with direct modulation DFB lasers. This is the first report of a 10 km range dynamic strain measurement with the theoretical repetition limit determined by the light flight time.

5.2 Frequency-swept pulse BOTDA

Figure 5-1 shows a schematic illustration of the proposed scheme. The Brillouin interaction occurs in a confined correlation region while the pump-probe frequency difference is given by the BFS in the pulses. With the proposed method, the frequency difference between test pulses is set at about the BFS. Moreover, both the pump and probe frequencies are swept linearly and synchronously. If there is a BFS change from BFS_1 to BFS_2, then the correlation region is slightly shifted, leading to a shift in the detection time of CBG peak Tp. The shift is calculated as the BFS change using the sweep rate. Author outline the basic principle of frequency-swept pulse BOTDA in the following sub-sections.

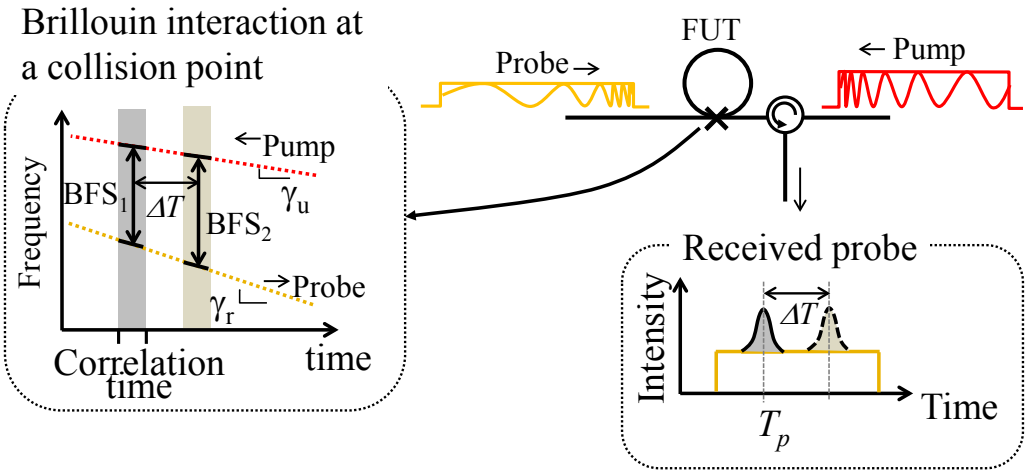

Fig. 5-1 Schematic illustration of proposed principle.

5.2.1 Acoustic wave generation with frequency-swept pulses

When the sweep rates are set at γ_u and γ_r [Hz/s] for the pump and probe, respectively, the pump-probe frequency difference at a collision point changes along with a relative sweep rate of $|\gamma_u-\gamma_r|$. The relative frequency difference at a point is shown by Eq. 5-1.

$$\nu(t) = \nu_{B0} + |\gamma_u - \gamma_r| t_p \quad (5\text{-}1),$$

where ν_{B0} is the initial frequency difference at a collision point, which is around BFS, and t_p is the existing time of the pump pulse at that point. Equation 1 means that the acoustic wave for the Brillouin interaction occurs with a relative frequency difference that changes dynamically with the relative sweep rate.

To describe the Brillouin interaction during the above process in detail, author consider it along with dynamic stimulated Brillouin scattering. Let $E_u(z, t)$, $E_r(z, t)$ and $\rho(z, t)$ be the electrical amplitudes of the pump and probe lights, and the acoustic wave amplitude, respectively, then the stimulated Brillouin scattering (SBS) can be represented by the following coupled equations [5-10];

$$\frac{1}{v}\frac{\partial E_u}{\partial t} + \frac{\partial E_u}{\partial z} = j\kappa E_r(z,t)\rho(z,t) \quad (5\text{-}2a)$$

$$\frac{1}{v}\frac{\partial E_r}{\partial t} - \frac{\partial E_r}{\partial z} = j\kappa E_u(z,t)\rho^*(z,t) \quad (5\text{-}2b)$$

$$\frac{\partial \rho}{\partial t} + \left(\frac{1}{2}\Gamma_B + j2\pi f_A(t)\right)\rho = j\Lambda E_u(z,t)E_r^*(z,t) \quad (5\text{-}2c)$$

where κ is an elasto-optic coefficient, Λ is an electrostrictive coupling coefficient, Γ_B is the linewidth of the acoustic wave spectrum, and $f_A(t)$ is the frequency shift of the pump/probe frequency offset with respect to the BFS of the fiber. $f_A(t)$ is shifted along with the second term of Eq. 5-1. When $t = 0$ is defined as the time at the beginning of the SBS, the stationary solution for the acoustic wave intensity can be given as follows

using the boundary conditions $E_s(z, t) = E_s$, and $\rho(z, t = 0) = 0$;

$$\rho(z,t,f_A) = j\Lambda E_s \int_0^{\Delta\tau_p} \frac{1}{2}\Gamma_B \exp\left[\left(-\frac{1}{2}\Gamma_B + j2\pi f_A\right)(t-t_p)\right] E_p(z,t_p)dt_p \tag{5-3}$$

The Brillouin gain after the collision is given by

$$G_B(z,f_A) = g_B(z)\rho(z,t,f_A)P_p(z) \tag{5-4}$$

where $g_B(z)$ is the peak Brillouin gain coefficient at $f_A = 0$, and $P_p(z)$ is the pump power at position z.

Figure 5-2 shows simulation results for the acoustic wave intensity obtained with Eq. 5-3. Here, γ in Fig. 5-2 represents the relative frequency sweep rate $|\gamma_u - \gamma_r|$. Figure 5-2 can be seen that the frequency-swept pump and probe induce the acoustic wave depending on the relative sweep rate γ. A faster relative sweep rate shapes the waveform with a lower intensity resulting in a degraded signal to noise ratio (SNR) and with a narrower full width at half maximum (FWHM) for the acoustic intensity leading to high BFS accuracy.

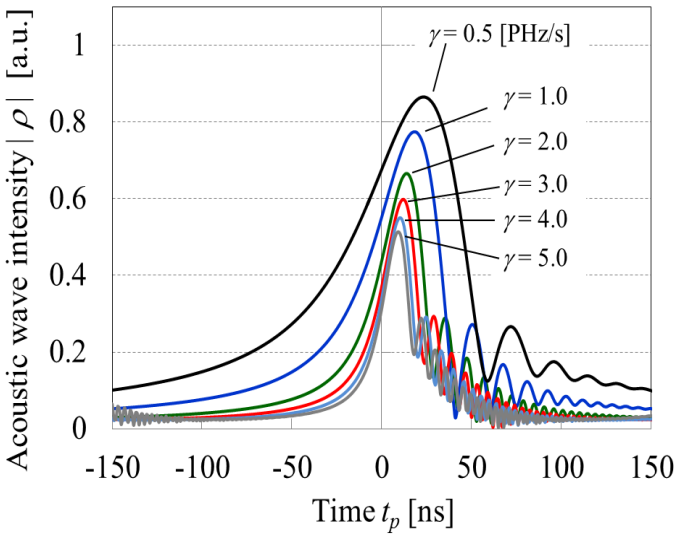

Fig. 5-2 Simulated result of acoustic wave in frequency-swept BOTDA.

5.2.2 CBG given by acoustic waves

Figure 5-3 is a schematic illustration of the Brillouin interaction between test pulses that generates the CBG on the probe. The states of the acoustic waves contributing the CBG differ with and without pump frequency sweeping. Figure 5-3 (a) shows a scheme with only a swept probe (i.e. γ_u=0). In contrast, in Fig. 5-3 (b) both a swept pump and probe are used. In both Fig. 5-3 (a) and (b), the acoustic wave appears mainly at each interaction position around z_0 where intending to obtain a diagnosis. Namely, the intensity of the acoustic waves decreases at peripheral positions. This is because the initial frequency difference between the pump and probe is a position dependent parameter. The CBG is the result of the total acoustic waves that the probe frequency component experiences when the pump pulse passes. Then, the acoustic waves induced on the periphery contribute crosstalk Brillouin gain, which reduces the spatial resolution. Note that in Fig. 5-3 (a), without pump sweeping, the peak intensity of the acoustic wave is just on the same time in probe pulse. In this scheme, the FWHM of CBG is expected to be almost the same as that of the acoustic wave determined by the relative sweep rate. On the other hand, in scheme involving both pump and probe sweeping shown in Fig. 5-3 (b), the region with a strong acoustic wave is strictly confined on the probe pulse. Compared with Fig. 5-3 (a), the initial frequency difference is changed more quickly, and then the peripheral acoustic waves around z_0 have relatively smaller peak intensities. Because of the pump frequency shift at each point, every acoustic wave has a peak at a different time during a collision. Although the correlated region is confined by using a swept pump, the FWHM of the CBG becomes wider than that of each acoustic wave shown in Fig. 5-2. The property of the FWHM of the CBG is

important because too wide a CBG is unsuitable for T_p measurement. Figure 5-4 shows the FWHM simulation results derived by Eq. 5-3. The simulated FWHM was calculated by the summation of the acoustic wave intensities, which gives Brillouin gain on a certain probe frequency component. The FWHM of the CBG appeared the narrowest band without pump sweeping (γ_u=0), and the width gradually decreased reaching several tens of nanoseconds with a relative sweep rate of over 1~3 Peta-Hertz/sec (PHz/s). The relative sweep rate should be faster along with the increment in the pump sweep rate if CBG is observed with a narrower FWHM.

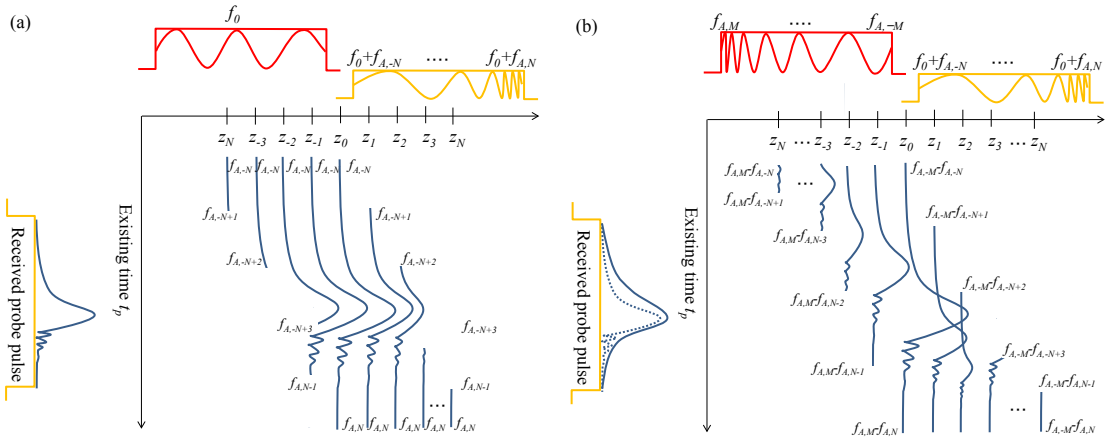

Fig. 5-3 Schematic illustration of acoustic wave in frequency-swept BOTDA (a) probe frequency-swept scheme (b) pump-probe frequency-swept scheme.

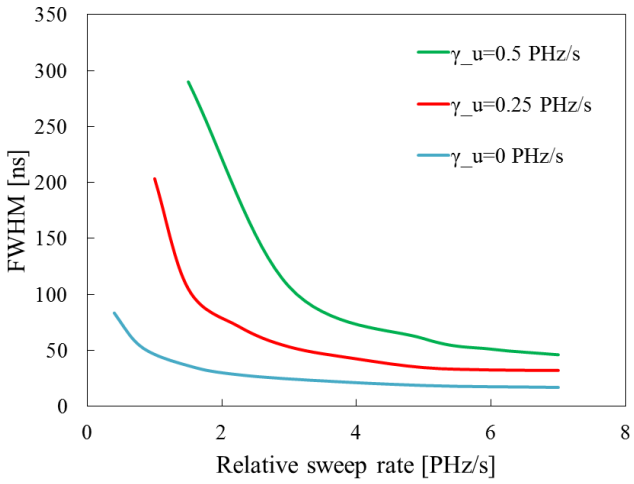

Fig. 5-4 Simulation results for FWHM of CBG related to the pump and probe sweep rate.

5.2.3 BFS acquisition with CBG

The proposed method is characterized by its BFS change detection scheme with a CBG shift in a time domain. If a dynamic strain is applied to the fiber section that causes a BFS change of ΔBFS, the detection time of the CBG peak T_p shifts slightly by ΔT. The time shift, ΔT, is given by

$$\Delta T = \frac{\Delta BFS}{|\gamma_u - \gamma_r|} \quad [\mathrm{s}]. \tag{5-5}$$

From Eq. 5-5, it was understood that the proposed method can measure the BFS change through monitoring the peak intensity in a time domain with a simple oscilloscope. The theoretical frequency resolution of the BFS change is determined by the sampling rate of the oscilloscope used to observe the CBG. The theoretical limited frequency resolution for BFS measurement, F_{res}, is expressed as below in Eq. 5-6;

$$F_{res} = \frac{|\gamma_u - \gamma_r|}{S} \quad [\mathrm{Hz}] \tag{5-6},$$

where S [sample points/s] is a sampling rate of the oscilloscope. To obtain frequency resolution with a sub-MHz order precision, a 10 giga-sample points/s or higher sampling rate oscilloscope would typically be needed when using a PHz-order sweep rate.

For more precise detection of the BFS change or to enable the use of a lower oscilloscope sampling rate, a quadrature fitting is very useful for interpolating plots. When a quadrature fitting is employed on the upper half of the CBG, the BFS error is expressed by Eq. 5-7. The equation is derived by deforming the original equation in the frequency domain proposed by Soto et al. in [5-11] into the time domain.

$$\sigma_{BFS} = \frac{|\gamma_u - \gamma_r|}{SNR}\sqrt{\frac{3}{4S}\cdot\Delta CBG} \quad [\text{Hz}] \tag{5-7}$$

where, *SNR* is the local signal to noise ratio on the trace of the CBG, and *ΔCBG* is the FWHM of the CBG in a time domain. According to Eq. 5-7, a narrow FWHM for the CBG and a slower sweep rate are better as regards suppressing BFS error.

5.2.4 Spatial resolution

The spatial resolution (*SR*) of the proposed method is determined by Eq. (8), and depends on the use of a larger pulse width for the pump and probe pulses, *W*, similar to the standard BOTDA spatial resolution [12].

$$SR = \frac{v_g W}{2} \tag{5-8}$$

Here, v_g is the light velocity in optical fiber. When there are multiple vibration points within the probe pulse width, CBGs appear simultaneously as a number of vibration points on the probe light pulse. And then, it becomes difficult to associate the time shift of CBG peaks with the CBG acquisition points. This feature will be mentioned again in the experimental results.

5.2.5 Effective sampling rate

The sampling rate is simply determined by the test pulse repetition rate because the peak time T_p is clearly measurable without averaging or test beam frequency scanning, whereas these procedures are generally unavoidable with other Brillouin-based schemes. T_p is mainly measured within a correlation time faster than the polarization fluctuation caused by the dynamic strain, thus the polarization noise is negligibly small. In a receiver system, time-domain analysis with an easy calculation is also useful for minimizing the measurement time. Quadrature fitting on the CBG with several hundreds of plots can be performed in real time, i.e. it can be finished within the test beam flight time. These features allow us to perform high-speed dynamic strain measurements up to the repetition rate limit determined by the length of the fiber.

The proposed method supports a random access distributed measurement by scanning the test pulse collision point by changing the pump-probe launching time delay. Here, the effective sampling rate drops by the value divided by the number of measurement points along a fiber. The entire distribution acquisition time T_s is expressed as Eq. 5-9 with fiber length L, and spatial resolution ΔL where M is the number of measurement points along a fiber. As a comparison, the acquisition time of BOTDA, $T_{s\text{-}BOTDA}$, is expressed as Eq. 5-10 and depends on the diagnosis bandwidth ΔBFS, frequency step δ and averaging time N.

$$T_s = \frac{2L}{v_g} \cdot M = \frac{2L}{v_g} \cdot \frac{L}{\Delta L} \tag{5-9}$$

$$T_{S-BOTDA} = \frac{2L}{v_g} \cdot \frac{\Delta BFS}{\delta} \cdot N \tag{5-10}$$

5.3 Experimental setup

Figure 5-5 shows the experimental setup. In this experiment, frequency-swept pump and probe beams were generated by distributed feedback laser diodes (DFB-LDs) with the injection current modulated by the linear swept intensity. The operating wavelength and linewidth of DFB-LDs were 1552 nm and less than 100 kHz, respectively. The injection currents into the LDs were modulated with a ramp shape generated by an arbitrary waveform generator. Since the laser drift during a measurement time of less than several seconds was negligibly small compared with the BFS accuracy, the setup did not employ the LD frequency lock function. The pump and probe lights were pulsed by acousto-optic modulators (AOMs) operated with signal synchronized with the LD injection current. Both the pulse widths (pump; W_u and probe; W_r) and the frequency sweep rates γ_u, γ_r were set at 1000 ns and 0.475, 3.385 PHz/s, respectively. Under these conditions, the *SR* was set at 100, according to Eq. 5-8. For the distribution measurement, the pulse widths W_u and W_r and frequency sweep rates γ_u, γ_r were set at 30 ns, 1 μs and 0 (without sweep) and 3.59 PHz/s, respectively. Those sweep rates were calculated from W_u and W_r and the beat spectrum bandwidth of the probe pulse and continuous reference beam monitored with an electrical spectrum analyzer. The sampling interval was set at 3 m by employing pulse repetition rates of 10 and 10.003 kHz for the pump and probe, respectively. The receiver system consisted of a single photodiode direct detection system and a 5 giga-sample/s, 10-bit digital oscilloscope, corresponding to the 0.58 MHz measurable resolution of the BFS without the quadrature fitting. The CBG was monitored, and its upper half consisted of 200 sampled plots (corresponding to 40 ns) that were fitted by a quadrature line to measure T_p. The

experimental setup was very simple because there was no need to set the original frequency difference between the pump and probe lights precisely.

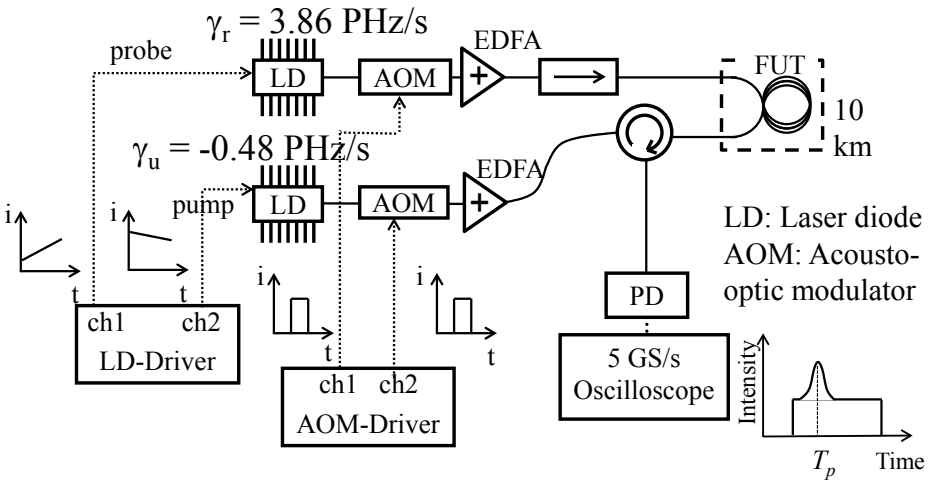

Fig. 5-5 Experimental set-up.

5.4 Experimental demonstrations

5.4.1 Configuration of fiber under test

Figure 5-6 shows the configuration of the fiber under test (FUT) -1, which consisted of 10 km of trunk fiber (SMF1) and a 20 m redundant part (SMF2 and SMF3) with a 1x2 optical switch to simulate dynamic strain. The optical path was changed with the switch, and the redundant part played the role of quasi-dynamic strain with a BFS difference of 59.7 MHz between SMF2 and SMF3 (corresponding to 1165 με, driven with a strain coefficient of 505.5 MHz/% [5-13]). As shown in Fig. 5-7, author prepared another FUT (FUT-2) for distributed sensing demonstration. That was consisted of two bobbins each wound with 5 km and a 20 m long fiber (SMF2 or -3) inserted between them to simulate a BFS variation.

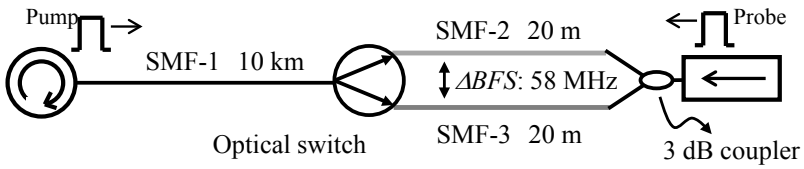

Fig. 5-6 Construction of FUT-1 with quasi-dynamic strain.

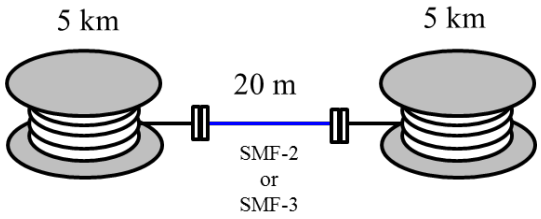

Fig. 5-7 Construction of FUT-2 with quasi-dynamic strain.

5.4.2 Experimental results

Figure 5-8 shows an experimental confirmation of the CBG FWHM, which was simulated as described in the previous section. The experimental results with various sweep rates shown as plots in Fig. 5-8 agreed with the simulated lines. The results proved that Eq. 5-2 expressed the dynamic stimulated Brillouin scattering.

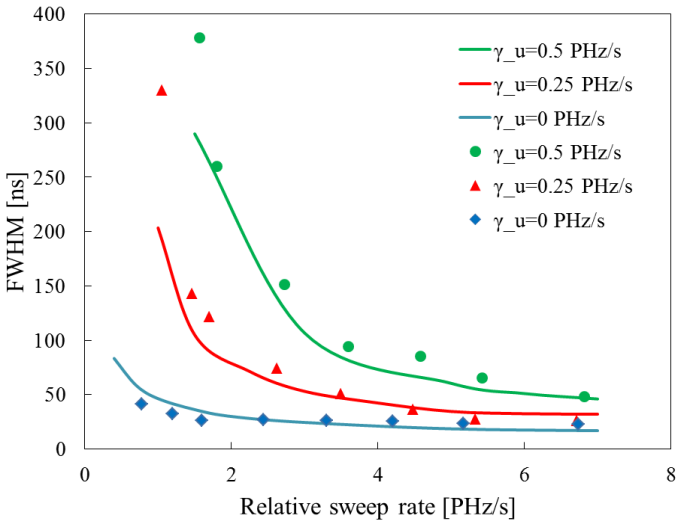

Fig. 5-8 Simulation (solid lines) and experiment (plots) results for FWHM of CBG related to the pump and probe sweep rate.

Figure 5-9 shows the CBG observed on the received probe pulse. The FWHM of the CBG was 58 ns, and the SNR was 10.1 without any averaging. According to Eq. 5-7, the theoretical BFS error was estimated at 1.1 MHz.

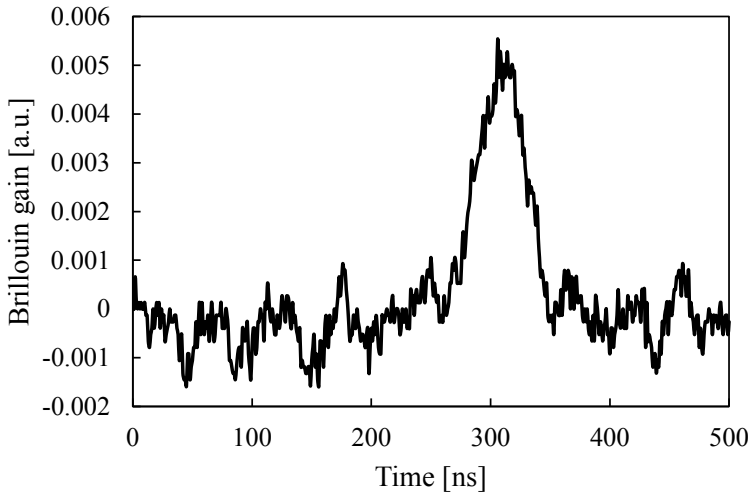

Fig. 5-9 Measurement result of CBG.

Figure 5-10 shows a measurement result with quadrature fitting. The results were obtained simultaneously using test beams with a 10 kHz repetition rate. (The theoretical limit determined by the flight time was 10 kHz for a 10 km long FUT.) Here, the optical switch ran at 20 Hz to simulate a 20 Hz dynamic strain. A 50 ms periodic BFS change of 56.7 MHz was observed with a BFS standard deviation of 1.3 MHz, corresponding to 26 με. Note that in this experiment, a vibration in 20 m section shorter than the 100 m spatial resolution was detected. This is because the condition of the FUT was ideal, namely a single vibration was applied to the fiber with a uniform BFS, and so the Brillouin interaction was strictly confined in the probe pulse. If there were multiple vibrations, resulting in multiple CBGs on the probe pulse, the BFS changes in the multiple CBG peaks could not be distinguished. In other words, author should use a shorter pulse width with enough remaining sensitivity to generate CBGs to achieve a more precise spatial resolution, otherwise, author should use a sensed fiber ideally connected to strain-free sections.

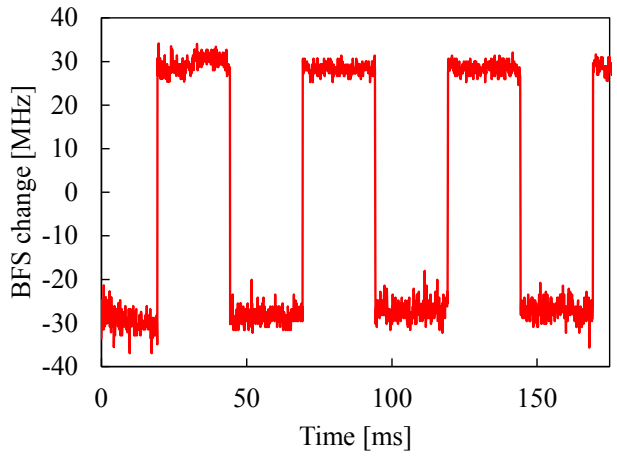

Fig. 5-10 Experimental result for 20 Hz quasi-dynamic strain measurement

Figure 5-11 evaluates the contribution of the quadrature fitting to the measurement accuracy. The figure shows the results obtained in the non-vibrational part (SMF-1 in Fig. 5-6) with and without quadrature fitting. The results show that the standard deviations of a static BFS were 1.7 and 5.4 MHz with and without fitting, respectively. The quadrature fitting resulted in 3.2 times better BFS accuracy. The reason for the discrepancy with the theoretical value (1.1 and 0.57 MHz) was assumed to be from laser instability and quantization noise with and without fitting, respectively.

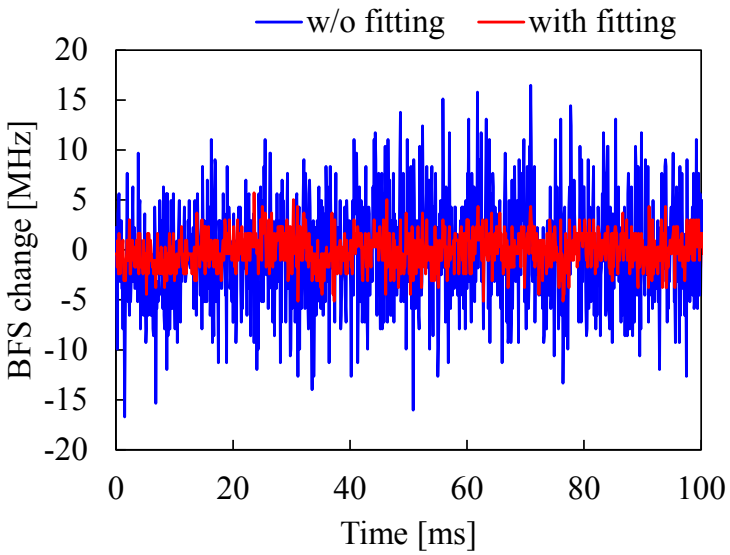

Fig. 5-11 Effectiveness of real-time quadrature fitting.

Figure 5-12 shows the overlaid pulses of 100 received probes to verify the electrical jitter. In the measurement, the standard deviation of the electrical jitter was 1.0 ns, which largely originated from a 250 MHz acousto-optic modulator (AOM). The 1.0 ns pulsed jitter degraded collision point repeatability was 10 cm.

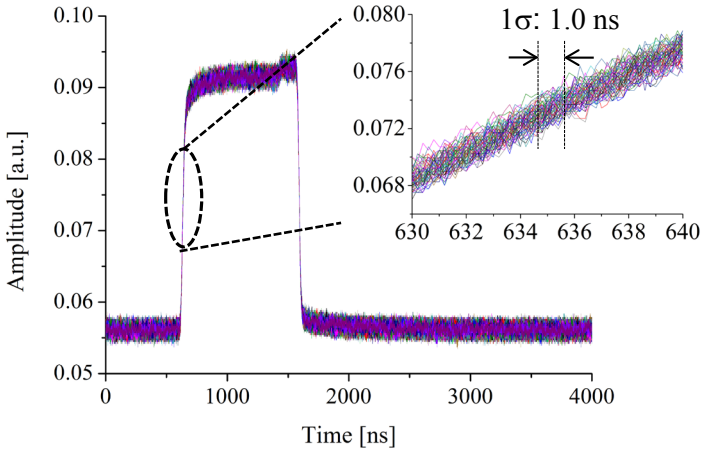

Fig. 5-12 The jitter of detected probe pulse.

Author mentioned the relationship between pulsed jitter and BFS measurement accuracy. Here, author investigates it employing pulse jitter compensation. The detected probe pulse edge was measured by using the power threshold, and compensated for the pulsed jitter. The power threshold was defined by a threshold point of 50 % of the pulse power level or three points at power levels of 10, 50, 90% for averaging. The measurement results were compared with the original result without jitter compensation. Figure 5-13 shows the results. The BFS accuracies (1σ) were unchanged by jitter compensation. This means that the pulsed jitter was not related to the BFS accuracy of the proposed method. The result shows that the requirement for electrical jitter on a pulsed modulator is not strictly in contrast to jitter on lasers.

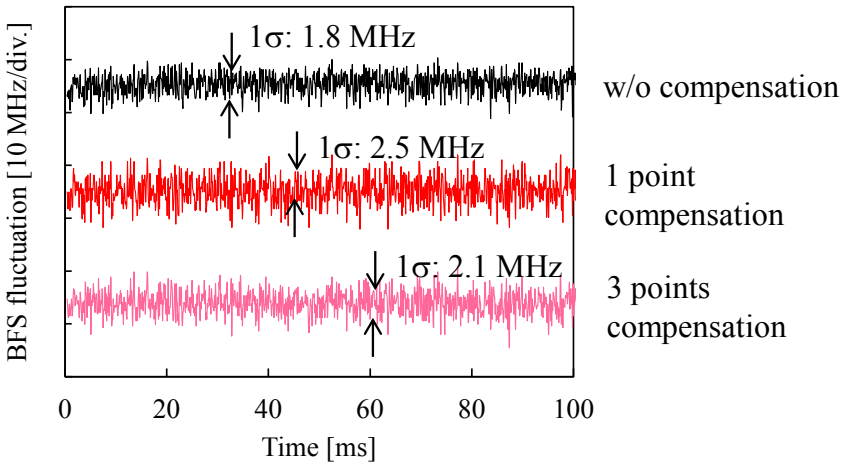

Fig. 5-13 Effect of pulsed jitter on BFS measurement accuracy. The jitters were compensated with threshold in leading edge of detected probe pulse.

Figure 5-14 shows the result obtained for a quasi-dynamic strain of 1 kHz to confirm the effective sampling rate for the measurement. One cycle of 10 kHz vibration was sampled at 10 points, corresponding to just 10 kilo-sample/s. This proved that the sampling rate of the proposed method was equal to the test beam repetition rate (10 kHz), which means it is unnecessary to consider any deterioration of the guard time or quadrature fitting calculation time. A fully real-time computation process was carried out during the measurement.

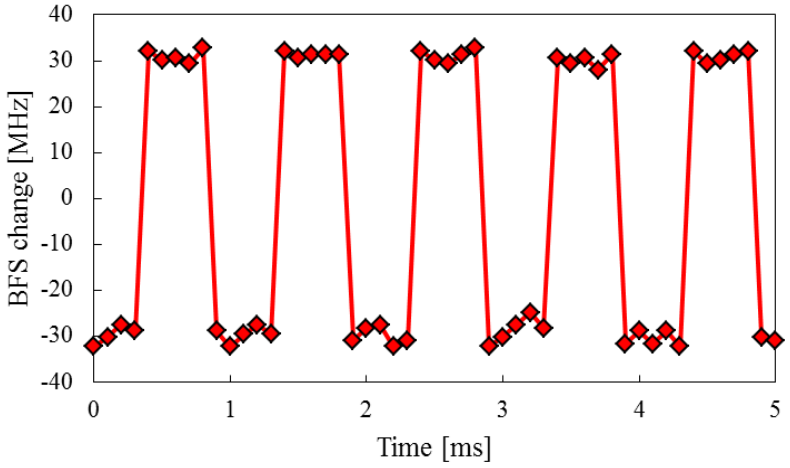

Fig. 5-14 Demonstration of 10 kilo-points/s dynamic strain measurement. The one cycles of 1 kHz quasi-dynamic strain were plotted with 10 points. This result proved the sampling rate of 10 kilo-points/s with real-time quadrature fitting.

Figure 5-15 shows demonstration results for a BFS distribution measurement. Figure 5-15 (a) clearly shows the BFS distribution with 1.8 MHz accuracy, corresponding to ±18 με. The discrepancy with the accuracy of 0.3 MHz estimated with Eq. 5-7 might be the result of electrical jitter in the injection current for the LDs. The result with the proposed method in Fig. 5-15 (b) was in good agreement with the BOTDR reference data shown in Fig. 5-15 (c). In the experiment, the acquisition time for the entire distribution T_s was 0.33 s. The fast acquisition time could be useful for dynamic strain measurements up to 1.5 Hz, which was a reciprocal number of $2T_s$. The faster vibration measurement was available in a shorter length fiber or with a deteriorated spatial resolution.

The proposed technique has the advantage of an acquisition time T_s for a wider BFS change bandwidth. The method was independent of the ΔBFS as shown in Eq. 5-9 because the frequency-swept probe typically had spectral bandwidth of over 1 GHz with a PHz-order frequency sweep rate and a μs-order probe pulse width W_r. In contrast, for the conventional BOTDA, the wider-band ΔBFS required additional time on $T_{S\text{-}BOTDA}$ as shown in Eq. 5-10. An additional advantage of T_s appeared with shorter length measurements (~10 km) because the T_s increases by L squared. Moreover, thanks to the pulse-pulse interaction and sufficient test beam power, the BFS error deterioration over distance was very small. In fact, a single shot measurement for even a distance of 40 km had a 1.9 MHz BFS accuracy, which was comparable to the value of 1.8 MHz for 10 km when using a high pump power of 21 dBm. Author believes that the proposed method would be a fast and simple BOTDA technique for practical use.

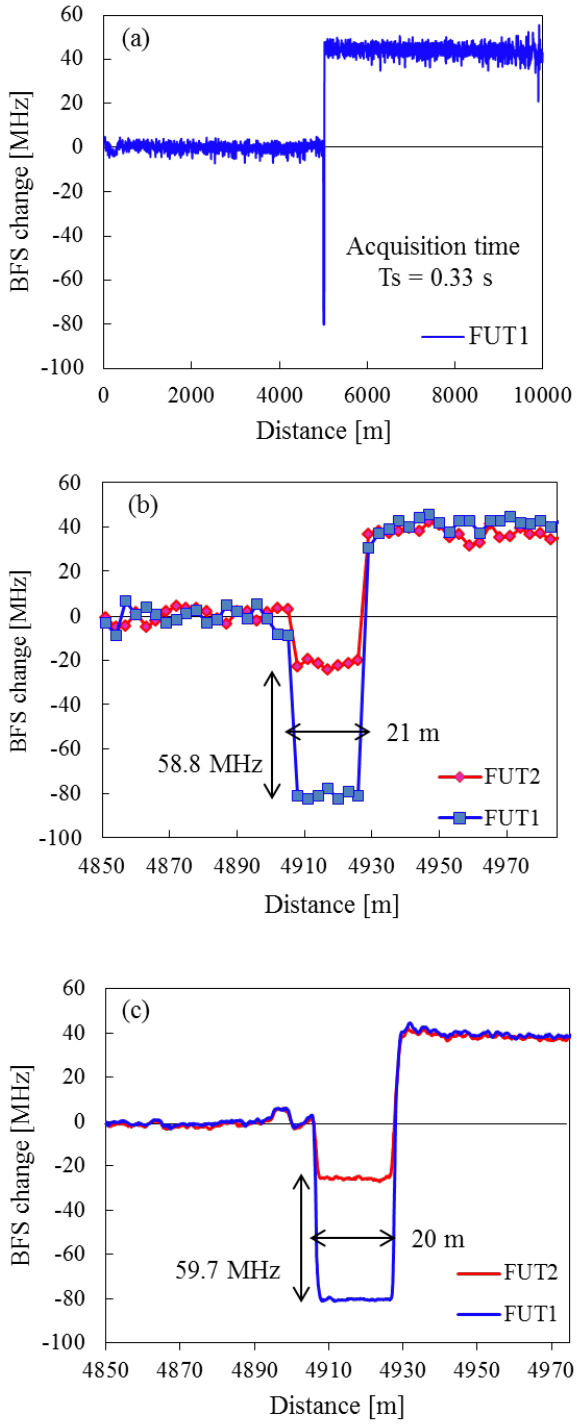

Fig. 5-15 Experimental demonstration result. (a) 10 km BFS distribution acquired in 0.33 s. (b) Enlarged figure at part with 20 m inserted fiber. (c) Reference date acquired by BOTDR for comparison.

5.5 Conclusion

Author demonstrated a fully real-time dynamic strain measurement with frequency-swept pulsed BOTDA in a 10 km sensing fiber. The time shift of the correlated Brillouin gain on the received probe pulse was simply translated into a BFS change with time domain analysis. Author investigated the CBG properties related to BFS accuracy and spatial resolution with experiments and simulations based on a dynamic acoustic wave. The proposed method was executed with a simple experimental setup compared with those used for Brillouin-based sensing schemes.

6 Summaries and conclusions

The main aim of this thesis was to develop an optical measurement technique for use with a branched fiber topology and based on end-reflection assisted Brillouin analysis (ERA-BA). By introducing a branch topology to the optical sensing network, the reliability and wiring scalability could be improved compared with the conventional unicursal writing topology, and thus allow its application range to be expanded. Moreover, as a loss measurement technology compatible with passive optical networks (PONs), which are the main distribution systems of the optical communication network, it was expected that the maintenance cost would be greatly reduced. And the applicability of ERA-BA in the field was demonstrated with in-service PONs. In addition, although there have been many previous reports on optical measurement techniques utilizing Brillouin scattering, I proposed a novel measurement technique that enables high-speed measurement with a highly simplified equipment setup. My proposed technique realized vibration measurement, and the successful results show the potential for expanding the Brillouin sensing application.

In chapter 2, I described the principle of Brillouin optical time domain analysis (BOTDA) and ERA-BA, which were the technical bases of this thesis. In chapter 3, I used ERA-BA as an optical fiber sensing technology corresponding to a branching topology. It achieved high-speed measurement employing a time-division multiplexed probe pulse train, and clarified an applicable area, which showed its superior sensitivity to standard BOTDA. In chapter 4, I conducted a field test using a prototype ERA-BA and confirmed its basic operation with deployed PONs. I also demonstrated that ERA-BA could be used as a fault detection technique even when the far-end reflectance

was very small, which assumes the detection of a broken fiber fault. In chapter 5, I proposed a novel BOTDA technique using a frequency-swept pulse, which was a suitable concept for application to ERA-BA. The proposed method realized a simplified setup and high-speed measurement.

The following summarizes the main results contained in chapters 3 to 5, which constitutes the main body of this thesis.

In chapter 3, by applying ERA-BA to optical fiber sensing technology, I realized high reliability and wiring scalability. The branched topology sensing network was especially suitable for a sensed area occupying 2 or 3 dimensions. I tuned ERA-BA for optical sensing and improved the measurement speed using a time-division multiplexed probe pulse train. The probe pulse train was only possible for use in temperature or strain sensing where the influence of pump depletion did not significantly affect the measurement result. As a result in the simulation and experiments, despite the existence of the branched loss that is inevitable in a branch topology, ERA-BA with a probe pulse train exhibited superior sensitivity to conventional BOTDA in a unicursal topology for most practical optical sensing network configurations (number of branches, distance). This is a major achievement of this thesis.

In chapter 4, I examined the applicability of ERA-BA for practical use in the telecommunication field. ERA-BA could be introduced as a loss distribution measurement technology for the branched fibers of PONs without making any changes to the network configuration. I confirmed the basic operation of ERA-BA in the field by performing an in-service test with deployed PONs. A variation in the Brillouin frequency shift (BFS) affects the loss measurement accuracy. Therefore, statistical data on BFS variation in the field were acquired. Furthermore, I acquired statistical field data

on the length and length difference of the branched fiber to set targets for spatial resolution and branched fiber identification resolution, which are important performance indices for ERA-BA. In addition, I performed experiments with an end-reflectance of -40 dB, which is the highest expected frequency at a broken fiber end, to show the wide applicability of ERA-BA for detecting broken fiber faults.

In chapter 5, I proposed a novel method that makes it possible to use a simple equipment setup and high-speed measurement by employing BOTDA with a frequency-swept pulse. By using a frequency-swept probe, a convex Brillouin gain could be obtained in a single shot, and BFS could be measured as the received time delay of the gain peak. This makes averaging and frequency analysis unnecessary. I used the proposed method to conduct a vibration measurement at an extremely high sample rate corresponding to the flight time of the test beam. The proposed method is unique in that it does not require the averaging time, has a simple equipment setup, and is unaffected by the polarization dependence of the Brillouin gain, which were major issues with the conventional optical measurement technologies using Brillouin scattering. The frequency-swept pulse method could be combined with ERA-BA described in chapters 3 and 4 in this thesis. So the advantages of ERA-BA, uniquely corresponding to the branched fiber configuration, would be emphasized by employing a frequency-swept pulse to simplify the equipment and a higher measurement speed.

Thus, this thesis contributes to the development of structural health monitoring (SHM) technology by improving the reliability and wiring scalability of optical sensing technology. In addition, it contributes to the accumulation of knowledge aimed at the practical application of remote testing, which is useful for the efficient maintenance of existing optical access networks. Furthermore, by using my proposed novel method, I

broadened the range of BOTDA applications including vibration measurement with the simultaneous realization of high-speed measurements and reduction of the equipment cost. These results can be expected to assist the development of Brillouin measurement techniques as widely applicable optical fiber sensing methods for SHM and telecommunication maintenance.

Acknowledgements

I express my sincere gratitude to Professor Fumihiko Ito of Shimane University for his guidance and encouragement throughout the course of this work. I also thank Professor Sumio Yano and Professor Masayuki Yokota of Shimane University, for their useful suggestions and guidance.

This thesis is based on research I performed at Nippon Telegraph and Telephone Corporation (NTT). I thank Mr. Yuki Sakuyama, Mr. Hiroaki Kubozono, and Mr. Hirofumi Amano who provided me with the opportunity to undertake the studies. I also thank Dr. Shigeru Tomita, Dr. Yuji Azuma, Dr. Kazuyuki Shiraki and Dr. Tetsuya Manabe for their kind encouragements and support throughout those studies.

I offer my sincere thanks to Dr. Kunihiro Toge and Mr. Hiroshi Takahashi for many helpful comments and discussions. Very special thanks to go my colleagues, Mr. Noriyuki Araki, Dr. Yusuke Koshikiya, Mr. Shingo Ohno for their great cooperation and fruitful discussions.

I also thank my family for supporting my life as a researcher.

References

Chapter1.

[1-1] Sohn H., Farrar C. R., Hemez F. M., Shunk D. D., Stinemates D. W., Nadler B. R., and Czarnecki J. J. “A review of structural health monitoring literature: 1996–2001,” Los Alamos National Lab., (2003).

[1-2] Farrar Charles R., and Keith Worden. "An introduction to structural health monitoring." Philosophical Transactions of the Royal Society of London A: Mathematical, Physical and Engineering Sciences, vol.365, no.1851, pp.303-315, (2007).

[1-3] Doebling S. W., Farrar C. R., Prime M. B., and Shevitz D. W., “Damage identification and health monitoring of structural and mechanical systems from changes in their vibration characteristics: a literature review,” Technical Report LA-13070-MS, Los Alamos National Lab., (1996).

[1-4] T. Horiguchi, K. Shimizu, T. Kurashima, M. Tateda, and Y. Koyamada. "Development of a distributed sensing technique using Brillouin scattering." J. lightw. Technol. Vol.13, no.7. pp.1296-1302, (1995).

[1-5] W. Li, X. Bao, Y. Li,and L. Chen, "Differential pulse-width pair BOTDA for high spatial resolution sensing." Optics express, vol.6, no.26, pp. 21616-21625, (2008).

[1-6] K. Kishida, C. Li, and K. Nishiguchi, “Pulse pre-pump method for cm-order spatial resolution of BOTDA,” Proc. SPIE 5855, 17th International Conference on Optical Fibre Sensors, 559, (2005).

[1-7] Y. Dong, X. Bao, and W. Li, "Differential Brillouin gain for improving the temperature accuracy and spatial resolution in a long-distance distributed fiber sensor,"

Appl. Opt., vo.48, no.22, pp.4297-4301, (2009).

[1-8] M. A. Soto, G. Bolognini, and F. D. Pasquale, "Long-range simplex-coded BOTDA sensor over 120km distance employing optical preamplification," Opt. Lett. Vol.36, no.2, pp. 232-234, (2011).

[1-9] E. Peter Carden, and P. Fanning, “Vibration Based Condition Monitoring: A Review,” Structural Health Monitoring, vol.3, no.4, pp.355-377, (2004).

[1-10] L. Wuilmart, V. Moeyaert, D. Daniaux, P. Megret, and M. Blondel, “A PC-based method for the localisation and quantization of faults in passive tree-structured optical networks using the OTDR technique,” in Proc. of IEEE

Conf. on Lasers and Electro-Optics Society, 2, 122–123, (1996).

[1-11] Y. Enomoto, H. Izumita, and M. Nakamura, “Highly developed fiber fault isolation technique for branched optical fibers of PONs using high spatial resolution OTDR and frequency domain analysis,” The Rev. of Laser Eng., vol.33, no. 9, (2005).

[1-12] N. Zou, Y. Namihira, C. Ndiaye, and H. Ito, “Fault location for branched optical fiber networks based on OFDR technique using FSF laser as light source,” in Proc. of Opt. Fiber Commun. Conf., 1–3, (2006).

[1-13] D. Iida, N. Honda, H. Izumita, and F. Ito, “Design of Identification Fibers With Individually Assigned Brillouin Frequency Shifts for Monitoring Passive Optical Networks,” J. lightw. Technol. Vol.25, no.5. pp.1290-1297, (2007).

[1-14] H. Takahashi, F. Ito, C. Kito, and K. Toge, "Individual loss distribution measurement in 32-branched PON using pulsed pump-probe Brillouin analysis," Opt. Express vol.21, no.6, pp.6739-6748 (2013).

[1-15] F. Ito, H. Takahashi, and K. Toge, "End-reflection Assisted Brillouin Measurement for PON Monitoring," in 2013 18th OptoElectronics and Communications

Conference, paper MS2_1, (2013).

[1-16] Derek Nesset, “NG-PON2 Technology and Standards,” J. lightw. Technol. Vol.33, no.5. pp.1136-1143, (2015).

[1-17] X. Bao, L. Chen, “Recent Progress in Brillouin Scattering Based Fiber Sensors,” Sensors, vol.11, no.4, pp.4152-4187, (2011).

Chapter 2.

[2-1] X. Bao, L. Chen, “Recent Progress in Brillouin Scattering Based Fiber Sensors,” Sensors, vol.11, no.4, pp.4152-4187, (2011).

[2-2] T. Horiguchi, and M. Tateda, “BOTDA - Nondestructive measurement of single-mode optical fiber attenuation characteristics using Brillouin interaction: Theory,” J. Lightw. Technol., Vol.7, no.8, pp.1170-1176, (1989).

[2-3] W. Li, X. Bao, Y. Li,and L. Chen, "Differential pulse-width pair BOTDA for high spatial resolution sensing." Optics express, vol.6, no.26, pp. 21616-21625, (2008).

[2-4] K. Kishida, C. Li, and K. Nishiguchi, “Pulse pre-pump method for cm-order spatial resolution of BOTDA,” Proc. SPIE 5855, 17th International Conference on Optical Fibre Sensors, 559, (2005).

[2-5] Y. Dong, X. Bao, and W. Li, "Differential Brillouin gain for improving the temperature accuracy and spatial resolution in a long-distance distributed fiber sensor," Appl. Opt., vo.48, no.22, pp.4297-4301, (2009).

[2-6] M. A. Soto, G. Bolognini, and F. D. Pasquale, "Long-range simplex-coded BOTDA sensor over 120km distance employing optical preamplification," Opt. Lett. Vol.36, no.2, pp. 232-234, (2011).

[2-7] T. Horiguchi and M. Tateda, "Optical-fiber-attenuation investigation using

stimulated Brillouin scattering between a pulse and a continuous wave," Opt. Lett. Vol.14, no.8, pp.408-410, (1989).

[2-8] F. Ito, H. Takahashi, K. Toge, and C. Kito, “End reflection assisted Brillouin measurement for PON monitoring,” OECC2013, paper MS2-1 (2013).

[2-9] H. Takahashi, F. Ito, C. Kito, and K. Toge, “Individual loss distribution measurement in 32-branched PON using pulsed pump-probe Brillouin analysis,” Opt. Express, vol.21, no.6, pp.6739-6748, (2013).

[2-10] G.P. Agrawal, Nonlinear Fiber Optics 4th edition, Academic Press, (2007).

[2-11] T. Kurashima, T. Horiguchi, and M. Tateda, “Thermal effects on Brillouin frequency shift in jacketed optical silica fibers,” Appl. Opt., Vol.29, no.15, pp. 2219-2222, (1990).

[2-12] T. Horiguchi, T. Kurashima and M. Tateda, “Tensile strain dependence of Brillouin frequency shift in silica optical fibers,” IEEE Photon. Tech. Lett., Vol.1, no.5, pp. 107-108, (1989).

[2-13] T. R. Parker, M. Farhadiroushan, V. A. Handerek, and A. J. Rogers, "Temperature and strain dependence of the power level and frequency of spontaneous Brillouin scattering in optical fibers," Opt. Lett., Vol.22, no.11, pp.787-789, (1997).

[2-14] Marcelo A. Soto and Luc Thévenaz, "Modeling and evaluating the performance of Brillouin distributed optical fiber sensors," Opt. Express, Vol.21, no.25, pp.31347-31366, (2013).

[2-15] T. Horiguchi, K. Shimizu, T. Kurashima, M. Tateda, and Y. Koyamada. "Development of a distributed sensing technique using Brillouin scattering." J. lightw. Technol. Vol.13, no.7. pp.1296-1302, (1995).

[2-16] “Optical fibre cable maintenance criteria for in-service fibre testing in access

networks," ITU-T L.66, (2007).

[2-17] Y. Koshikiya, N. Araki, H. Izumita, and F. Ito, "Newly Developed Optical Fiber Line Testing System Employing Bi-Directional OTDRs for PON and In-Service Line Testing Criteria," IEICE TRANSACTIONS on Communications, Vol.E90-B, no.10, pp.2793-2802, (2007).

Section 3.

[3-1] T. Horiguchi, T. Kurashima, and M. Tateda, "A technique to measure distributed strain in optical fibers," IEEE Photon. Technol. Lett. vol. 2, no. 5, pp. 352-354 (1990).

[3-2] X. Bao, D. J. Webb, and D. A. Jackson, "22-km distributed temperature sensor using Brillouin gain in an optical fiber," Opt. Lett., vol. 18, no. 7, pp. 552-554 (1993).

[3-3] M. Niklès, L. Thévenaz, and P. Robert, "Simple distributed fiber sensor based on Brillouin gain spectrum analysis," Opt. Lett., vol. 21, no. 10, pp. 758-760 (1996).

[3-4] K. Hotate and T. Hasegawa, "Measurement of Brillouin gain spectrum distribution along an optical fiber using a correlation-based technique - Proposal, experiment and simulation -," IEICE Trans. Electron. E83-C, pp. 405-412, (2000).

[3-5] K. Shimizu, T. Horiguchi, and Y. Koyamada, "Measurement of distributed strain and temperature in a branched optical fiber network by use of Brillouin optical time-domain reflectometry," Opt. Lett. vol. 20, no. 5, pp.507-509 (1995).

[3-6] F. Ito, H. Takahashi, K. Toge, and C. Kito, "End reflection assisted Brillouin measurement for PON monitoring," OECC2013, paper MS2-1 (2013).

[3-7] H. Takahashi, F. Ito, C. Kito, and K. Toge, "Individual loss distribution measurement in 32-branched PON using pulsed pump-probe Brillouin analysis," Opt. Express, vol. 21, no. 6, pp. 6739-6748 (2013).

[3-8] C. Kito, F. Ito, H. Takahashi, and K. Toge, “End-reflection assisted time domain Brillouin sensing with a novel probe pulse arrangement for branched fiber,” Proc. SPIE 9157, 23rd International Conference on Optical Fibre Sensors, 91576F (2014).

[3-9] Marcelo A. Soto, and Luc Thévenaz, “Modeling and evaluating the performance of Brillouin distributed optical fiber sensors,” Optics Express, vol. 21,Issue 25,pp. 31347-31366 (2013).

Section 4.

[4-1] L. Wuilmart, V. Moeyaert, D. Daniaux, P. Megret, and M. Blondel, “A PC-based method for the localisation and quantization of faults in passive tree-structured optical networks using the OTDR technique,” Proc. of IEEE Conf. on Lasers and Electro-Optics Society, 2, pp. 122-123, (1996).

[4-2] L. Laferriere, M. Saget, and A. Champavere, “Original method for analyzing multipaths networks by OTDR measurement,” Proc. of Optical Fiber Commun. Conf., pp. 99-101, (1997)

[4-3] Y. Enomoto, H. Izumita and M. Nakamura, “Highly developed fiber fault isolation technique for branched optical fibers of PONs using high spatial resolution OTDR and frequency domain analysis,” The Rev. of Laser Engineering, 33, No. 9, (2005)

[4-4] F. Ito, H. Takahashi, K. Toge, and C. Kito, “End reflection assisted Brillouin measurement for PON monitoring,” OECC2013, paper MS2-1 (2013)

[4-5] H. Takahashi, F. Ito, C. Kito, and K. Toge, “Individual loss distribution measurement in 32-branched PON using pulsed pump-probe Brillouin analysis,” Opt. Express, vol. 21, no. 6, pp. 6739-6748 (2013)

[4-6] T. Horiguchi, T. Kurashima, and M. Tateda, “A technique to measure distributed

strain in optical fibers," IEEE Photon. Technol. Lett., vol. 2, no. 5, pp. 352-354 (1990)

[4-7] T. Kurashima, T. Horiguchi, and M. Tateda, "Distributed-temperature sensing using stimulated Brillouin scattering in optical silica fibers," Opt. Lett., vol. 15, no.18, pp. 1038-1040 (1990)

[4-8] M. Tateda, T. Horiguchi, T. Kurashima, and K. Ishihara, "First measurement of strain distribution along field-installed optical fibers using Brillouin spectroscopy," J. Lightw. Technol., vol. 8, no. 9, pp. 1269-1272 (1990)

[4-9] Recommendation ITU-T G.652, "Characteristics of a single-mode optical fibre and cable." (2003)

[4-10] Recommendation ITU-T G.657, "Characteristics of a bending-loss insensitive single-mode optical fibre and cable for the access network." (2012)

[4-11] H. Takahashi, X. Fan, Y. Koshikiya, and F. Ito, "Distributed 32-branched PON Measurement Using Pulsed Pump-Probe Brillouin Analysis," ECOC2012 Technical Digest, P1.06, (2012).

[4-12] Recommendation ITU-T L.66, "Optical fibre cable maintenance criteria for in-service fibre testing in access networks." (2007)

[4-13] Recommendation ITU-T L.42, "Extending optical fibre solutions into the access network." (2003)

[4-14] F. P. Kapron, B. P. Adams, E. A. Thomas, and J. W. Peters, "Fiber-Optic Reflection Measurements Using OCWR and OTDR Technique," J. Lightwave Technol., Vol. 7, No. 8 (1989).

[4-15] Y. Enomoto, H. Izumita, K. Mine, S. Uruno, and Nobuo Tomita, "Design and performance of novel optical fiber distribution and management system with testing functions in central office," J. Lightw. Technol., vol. 29, no. 12, pp. 1818-1834 (2011)

[4-16] H. Takahashi, K. Toge, and F. Ito, “Centralized monitoring of true splice loss in PON including MFD mismatched fibres,” ECOC2013, We.2.F.2 (2013)

Section 5.

[5-1] T. Horiguchi et al., “A Technique to Measure Distributed Strain in Optical Fibers,” IEEE Photon. Technol. Lett., Vol. 2, no. 5, p. 352 (1990).

[5-2] K. Hotate et al., “Measurement of Brillouin Gain Spectrum Distribution along an Optical Fiber Using a Correlation-Based Technique - Proposal, Experiment and Simulation -, ” IEICE Trans. Electron. E83-C, p. 405 (2000).

[5-3] R. Bernini et al., "Dynamic strain measurement in optical fibers by stimulated Brillouin scattering," Opt. Lett. Vol.34, no.17, p.2613-2615 (2009)

[5-4] Y. Peled et al., “Slope-assisted fast distributed sensing in optical fibers with arbitrary Brillouin profile,” Opt. Express Vol. 19, no. 21, 19845 (2011).

[5-5] X. Tu et al., “Performance analysis of slope-assisted dynamic BOTDA based on Brillouin gain or phase-shift in optical fibers,” J. Opt. Vol. 17, no. 10, 105503 (2015).

[5-6] C. Zhang et al., “5,000 points/s High-Speed Random Accessibility of Brillouin Optical Correlation Domain Analysis for Dynamic Strain Measurement at Arbitrary Multiple Points along a Fiber,” Proc. Light, Energy and the Environment, JW6A.1 (2014).

[5-7] X. Bao et al., “Monitoring the distributed impact wave on a concrete slab due to the traffic based on polarization dependence on stimulated Brillouin scattering,” Smart Mater. Struct., Vol. 17, No. 1, 015003 (2007).

[5-8] Y. Mizuno et al., “High-performance Brillouin optical correlation-domain reflectometry,” Proc. of SPIE Vol. 9634 (2015).

[5-9] K. Koizumi et al., “High-Speed Distributed Strain Measurement using Brillouin Optical Time-Domain Reflectometry Based-on Self-Delayed Heterodyne Detection,” Proc. of ECOC2015, P.1.7 (2015).

[5-10] G. P. Agrawal, “Nonlinear Fiber Optics,” 4th ed., Springer.

[5-11] M. A. Soto et al., “Modeling and evaluating the performance of Brillouin distributed optical fiber sensors,” Opt. Express, Vol. 21, No. 25, 31347 (2013).

[5-12] T. Horiguchi et al., “Development of a Distributed Sensing Technique Using Brillouin Scattering,” J. Lightw. Technol., Vol. 13, no. 7, p. 1296 (1995).

[5-13] L. Thévenaz, “Brillouin distributed time-domain sensing in optical fibers: state of the art and perspectives,” Front. Optoelectron. China Vol. 3, no. 1, p. 13 (2010).

List of publications

Papers related to this thesis

1. C. Kito, H. Takahashi, K. Toge, and T. Manabe “Dynamic Strain Measurement on 10 km Fiber with Frequency-swept Pulse BOTDA,” IEEE/OSA J. Lightwave Technol. Vol. 35, No. 9, pp.1738-1743 (2017).

2. C. Kito, H. Takahashi, K. Toge, S. Ohno, and T. Manabe “Field measurement of PON branches with end-reflection assisted Brillouin analysis,” IEEE/OSA J. Lightwave Technol. Vol. 34, No. 19, pp.4454-4459 (2016).

3. C. Kito, F. Ito, H. Takahashi, K. Toge, and T. Manabe, "Robust and high-Sensitivity Brillouin time-domain sensing with branched-fiber configuration," IEEE/OSA J. Lightwave Technol. Vol. 33, No. 20, pp.4291-4296 (2015).

Letter related to this thesis

1. C. Kito, H. Takahashi, K. Toge, and F. Ito, “Loss distribution measurement of broken PON by end-reflection-assisted Brillouin analysis,” IEEE Photonics Technology Letters, Vol. 26, No. 11, pp. 1139-1141 (2014).

International conferences related to this thesis

1. C. Kito, H. Takahashi, K. Toge, and T. Manabe, “Simplified and fast acquirable BOTDA with frequency-swept probe pulse,” 25th International Conference on Optical Fiber Sensors (OFS-25), Jeju, April. 2017, Proc. SPIE, Vol. 10323, pp. 343.

2. C. Kito, H. Takahashi, and K. Toge, and T. Manabe, “High-speed Dynamic Strain Measurement Based on Frequency-swept Pulsed BOTDA,” 42nd European Conference and Exhibition on Optical Communications (ECOC2016), Düsseldorf, Sep. 2016, Paper Th.2.P2.

3. C. Kito, H. Takahashi, K. Toge, and T. Manabe, “First field demonstration of end-reflection assisted Brillouin analysis for in-service loss monitoring of branched fibers in PONs,” 24th International Conference on Optical Fiber Sensors (OFS-24), Curitiba, Sep. 2015, Proc. SPIE, Vol. 9634, pp. 96341V.

4. C. Kito, F. Ito, H. Takahashi, and K. Toge, “End-reflection assisted time domain Brillouin sensing with a novel probe pulse arrangement for branched fiber,” 23rd International Conference on Optical Fiber Sensors (OFS-23), Santander, July 2014, Proc. SPIE, Vol. 9157, pp. 91576F.

Domestic conferences related to this thesis

国内講演

光ファイバ応用技術研究会

1. 鬼頭千尋，高橋央，戸毛邦弘，真鍋哲也，“周波数掃引プローブパルスの利用による BOTDA の簡易化と高速化”，信学技報，ISSN 0913-5685，2017 年 5 月.

2. 鬼頭千尋，高橋央，戸毛邦弘，真鍋哲也，“周波数掃引パルスによるブリルアン散乱を利用した動的歪測定”，信学技報，OFT2016-295，41-44，2016 年 11 月.

3. 鬼頭千尋，高橋央，戸毛邦弘，真鍋哲也，“実線路における遠端反射ブリルアン利得解析法を用いた分岐下部モニタリングの実証”，信学技報，OFT2015-23，39-42，2015 年 8 月.

4. 鬼頭千尋，高橋央，戸毛邦弘，真鍋哲也，伊藤文彦，“断線故障モニタリングに対する遠端反射ブリルアン解析法の適用性”，信学技報，OFT2014-40，15-18，2014 年 11 月.

5. 鬼頭千尋，伊藤文彦，高橋央，戸毛邦弘，真鍋哲也，“複数プローブ光を用いた遠端反射ブリルアン利得解析法による高信頼分岐光ファイバセンシング”，信学技報，OFT2014-29，33-38，2014 年 10 月.

電子情報通信学会

1. 鬼頭千尋，高橋央，戸毛邦弘，真鍋哲也，“周波数掃引プローブパルスを用いた簡易型BOTDA”，2017 年電子情報通信学会総合大会，B-13-17，2017 年 3 月.

2. 鬼頭千尋，高橋央，戸毛邦弘，真鍋哲也，“周波数掃引パルスを用いた BOTDA による動的歪測定”，2016 年電子情報通信学会ソサイエティ大会，B-13-4，2016 年 9 月.

3. 鬼頭千尋，高橋央，戸毛邦弘，大野槙悟，真鍋哲也，“遠端反射ブリルアン利得解析法による分岐下部損失フィールド測定”，2016 年電子情報通信学会総合大会，B-13-15，2016 年 3 月.

4. 鬼頭千尋，伊藤文彦，高橋央，戸毛邦弘，真鍋哲也，“複数プローブパルスを用いた分岐光ファイバセンサの適用領域”，2015 年電子情報通信学会ソサイエティ大会，B-13-16，2015 年 9 月.

5. 鬼頭千尋，高橋央，戸毛邦弘，真鍋哲也，“複数プローブパルスを用いた遠端反射ブリルアン利得解析法におけるポンプディプレッション”，2015 年電子情報通信学会総合大会，B-13-34，2015 年 3 月.

6. 鬼頭千尋，伊藤文彦，高橋央，戸毛邦弘，真鍋哲也，“遠端反射ブリルアン利得解析法による分岐光ファイバセンサ”，2014 年電子情報通信学会ソサイエティ大会，B-13-1，2014 年 9 月.

7. 鬼頭千尋，高橋央，戸毛邦弘，伊藤文彦，“遠端反射ブリルアン解析法による断線故障モニタリング”，2014 年電子情報通信学会総合大会，B-13-32，2014 年 3 月.

8. 鬼頭千尋，高橋央，戸毛邦弘，伊藤文彦，“遠端反射ブリルアン解析法における遠端反射率に関する検討”，2013 年電子情報通信学会ソサイエティ大会，B-13-42，2013 年 9 月.

Others

Paper

- 鬼頭千尋，古敷谷優介，荒木則幸，伊藤文彦，“光設備管理のための波長多重型多ビット光 ID 素子”，電子情報通信学会論文誌 Vol. J95-B, No.12, pp. 1607-1615 (2012).

International conference

- C. Kito, F. Ito, H. Takahashi, and K. Toge, “Frequency-code multiplexed end reflection assisted Brillouin analysis for monitoring PONs,” 39th European Conference on Optical Communication (ECOC 2013), London, Sept. 2013, paper We.2.F.3

Domestic conference

- 鬼頭千尋，伊藤文彦，高橋央，戸毛邦弘，“周波数コーディングパルス列を用いた遠端反射ブリルアン利得解析によるスプリッタ下部測定技術”，信学技報，OFT2013-17，21-24，2013 年 8 月.

- 鬼頭千尋，高橋央，戸毛邦弘，伊藤文彦，“周波数コーディング法を用いたスプリッタ下部ファイバ個別損失分布測定技術の提案”，2013 年電子情報通信学会総合大会，B-13-23，2013 年 3 月.

- 鬼頭千尋，古敷谷優介，荒木則幸，伊藤文彦，“SC コネクタ内に実装した波長多重型 FBG による光 ID 素子”，2012 年電子情報通信学会総合大会，B-13-28，2012 年 3 月